CHEMISTRY
A EUROPEAN JOURNAL

DOI: 10.1002/chem.201102868

Tetrathiafulvalene–Oligo(*para*-phenyleneethynylene) Conjugates: Formation of Multiple Mixed-Valence Complexes upon Electrochemical Oxidation

Šárka Lipnická,[a] Martin Bělohradský,[a] Viliam Kolivoška,[b] Lubomír Pospíšil,*[a, b] Magdaléna Hromadová,[b] Radek Pohl,[a] Jana Vacek Chocholoušová,[a] Jaroslav Vacek,[a] Jan Fiedler,[b] Irena G. Stará,[a] and Ivo Starý*[a]

Dedicated to Dr. Jiří Závada on the occasion of his retirement

Abstract: Short monodisperse oligo(*para*-phenyleneethynylene) (*p*OPE) units bearing laterally attached tetrathio-substituted tetrathiofulvalene (TTF) units have been synthesised from functionalised aromatic building blocks by using the Sonogashira cross-coupling methodology. The unusual redox properties of these TTF–*p*OPE conjugates were observed by employing electrochemical methods, such as cyclic voltammetry and exhaustive electrolysis. We found that formally one half of the TTF units in the *p*OPE monomer **1**, dimer **2**, and trimer **3** (with 2, 4, and 6 TTF units, respectively) are electrochemically silent during the first-step oxidation at 0.49 V. We propose the formation of persistent mixed-valence complexes from the TTF and $TTF^{+\bullet}$ units present in an equal ratio. Such mixed-valence dyads (single or multiple in the partially oxidised **1**–**3**) exhibit an unusual stability towards oxidation until the potential of the second oxidation at 0.84 V is achieved. This finding suggests that below this potential the oxidation of the respective mix-valence complexes is extremely slow.

Keywords: cross-coupling • donor–acceptor systems • electrochemistry • oligomers • tetrathiafulvalene

Introduction

Functionalised monodisperse oligo(*para*-phenyleneethynylene)s[1] (*p*-OPEs) have recently attracted significant attention for manifold reasons, namely, they can be synthesised in a straightforward way by employing the reliable Sonogashira coupling methodology[2] optionally connected with an effective convergent/divergent approach,[3] they have been intensively studied as π-conjugated molecular wires,[4] and they have been cleverly used as shape-persistent, easy-to-make molecular scaffolds.[5] The effective synthetic methodology has allowed for the preparation of monodisperse OPEs, the length of which can range from a dimer up to 23-mer that reaches 15 nm.[6] The inner *para*-phenylene unit of the OPEs has been described as bearing alkyl,[5a,7] alkoxyl,[8] perfluoroalkyl,[9] aryl,[10] alkenyl,[11] alkynyl,[12] cyano,[9,13] halo,[9,14] nitro,[15] amino,[16] hydroxy,[17] diarylboranyl,[18] carbonyl,[19] alkoxycarbonyl,[20] carboxyl,[21] alkoxy(dialkyl)silyl,[18a] or 1,3-dithiol-2-ylidenemethyl[22] groups. In the realm of the polymeric *p*OPEs,[23] other structural variations, such as pendant phosphonate, sulfonate, bis-alkylammonium solubilising substituents,[24] or attached biomolecules have even been found.[25] Thus, a large portfolio of the *p*OPEs bearing diverse functionalities has already been synthesised and various physicochemical properties of these π-conjugated rods have been studied. However, there are only scattered examples of monodisperse *p*OPEs conjugated with tetrathiofulvalene (TTF) moieties[26] or their parts[22] and, to the best of our knowledge, there has been no systematic study on this subject.

Within a long-term program focused on the development of new zipper-type multiple donor–acceptor (D–A) interactions, we turned our attention to the short *p*OPE rods equipped laterally with TTF units. Importantly, the concept of the zipper assembly has already been demonstrated by Matile and Sakai in an intriguing series of reports,[27] in which they have recently described the formation of *n*/*p*-heterojunction photosystems containing interdigitated *p*OPE chromophores (along with *para*-oligophenyl moieties) bearing pendant and electronically tuned naphthalenediimide

---

[a] Š. Lipnická, Dr. M. Bělohradský, Assoc. Prof. Dr. L. Pospíšil,
Dr. R. Pohl, Dr. J. V. Chocholoušová, Dr. J. Vacek, Dr. I. G. Stará,
Dr. I. Starý
Institute of Organic Chemistry and Biochemistry, v.v.i.
Academy of Sciences of the Czech Republic
Flemingovo nám. 2, 16610 Prague 6 (Czech Republic)
Fax: (+)420-220 183 133
E-mail: stary@uochb.cas.cz

[b] V. Kolivoška, Assoc. Prof. Dr. L. Pospíšil, Dr. M. Hromadová,
Dr. J. Fiedler
J. Heyrovský Institute of Physical Chemistry, v.v.i.
Academy of Sciences of the Czech Republic
Dolejškova 3, 18223 Prague 8 (Czech Republic)
Fax: (+)420-286 582 307
E-mail: lubomir.pospisil@jh-inst.cas.cz

Supporting information for this article is available on the WWW under http://dx.doi.org/10.1002/chem.201102868.

(NDI) chromophores. By following this general paradigm of supramolecular assembly, which has so far scarcely been studied relative to, for instance, hydrogen-bonding-controlled self-organisation,[28] promising highly ordered functional materials might be envisaged in connection with photovoltaics and molecular electronics or the development of new programmable binding motifs.

Our interest in monodisperse *p*OPEs with tethered TTF units stems from the unique redox properties of TTF. The discovery of the parent TTF molecule in 1970[29] initiated considerable efforts in the synthesis and application of this simple compound and its derivatives.[30] Homogeneous or heterogeneous reversible oxidation of the nonaromatic TTF to a half-aromatic radical cation TTF$^{+\bullet}$ and a fully aromatic dication TTF^{2+} makes this redox system an attractive building block for larger molecules and functional materials.[31] Upon generating the radical ion TTF$^{+\bullet}$ from electroneutral closed-shell TTF, an original electron donor (D) is converted into an electron acceptor (A), as a consequence of which the formation of a D–A complex represented by the [(TTF)$_2$]$^{+\bullet}$ mixed-valence dyad (π dimer) might be anticipated. However, the interaction energy between the filled and half-filled HOMO orbitals of the individual components is small, which results in the intermolecular mixed-valence TTF complexes in solution being elusive.[32,33] These complexes can be detected only under specific circumstances.[34] Providing that this weak association is supported by additional forces such as an intermolecular π–π interactions,[32] physical constriction inside a cage structure,[35] a covalent junction between the respective TTF units,[36] or a preorganised zipper-type interaction,[37] the rare mixed-valence complex of the [(TTF)$_2$]$^{+\bullet}$ structure might be observed. Moreover, TTF$^{+\bullet}$ can spontaneously self-associate to form a diamagnetic [(TTF)$_2$]$^{2+}$ dication (π dimer).[34] The question of whether the TTF$^{+\bullet}$ moieties coexist independently under partial oxidation along with the parent TTF or the π dimers such as [(TTF)$_2$]$^{+\bullet}$ or [(TTF)$_2$]$^{2+}$ are formed relates to the solid-state conductivity of *p*-doped TTF stacks. The strong electronic coupling inside the [(TTF)$_2$]$^{+\bullet}$ dyad leads to the π-electron delocalisation necessary for effective charge propagation along the TTF stacks, whereas any strong π bonding within the [(TTF)$_2$]$^{2+}$ ion results in nonconducting states.[34]

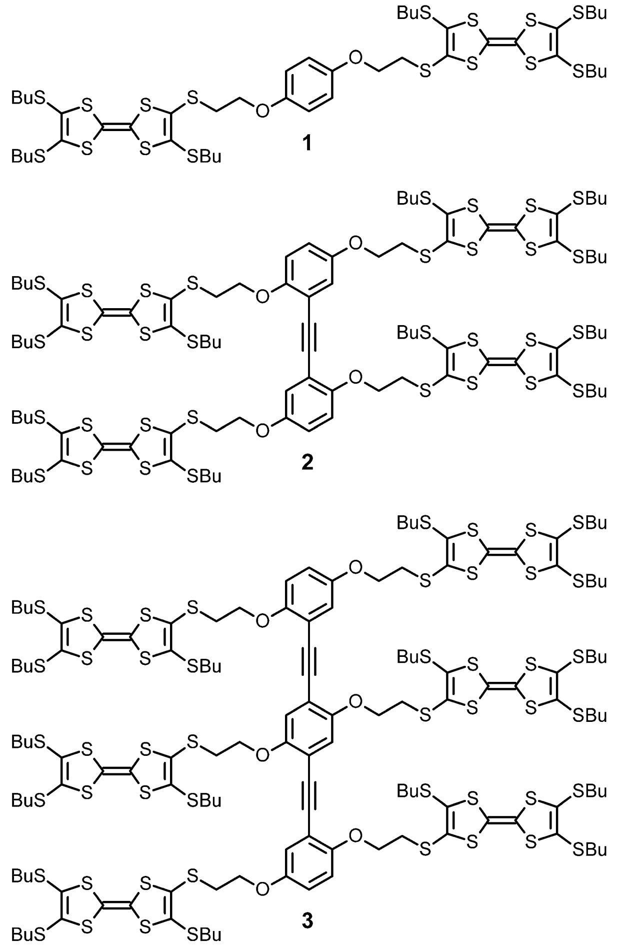

Figure 1. The models of the multiple TTF–*p*OPE conjugates **1**–**3**.

Herein, we report on the synthesis and physicochemical properties of the new TTF–*p*OPE conjugates **1**–**3** (Figure 1). These short double-sided combs bear two, four, or six electroactive TTF groups laterally attached to the central phenylene unit or *p*OPE rod. In particular, we studied their intriguing redox properties to observe the spontaneous formation of mixed-valence [(TTF)$_2$]$^{+\bullet}$-type complexes. Such a multiple D–A interaction might give rise to new interlaced supramolecular assemblies that bridge the gap between the solution and solid-state realms.

Results and Discussion

Synthesis of the TTF–*p*OPE conjugates: The model monomer **1** bearing two TTF units was synthesised in a straightforward way from the known dibromide **4**[38] and (2-cyanoethyl)sulfanyl TTF derivative **5**[39] by following the procedure published by Nielsen and co-workers[39] (Scheme 1). Upon the treatment of **5** with cesium hydroxide, the labile 2-cyanoethyl group was easily removed and the resulting thiolate anion readily displaced the bromine atoms in **4** to provide **1** in an acceptable yield after its purification by liquid chromatography.

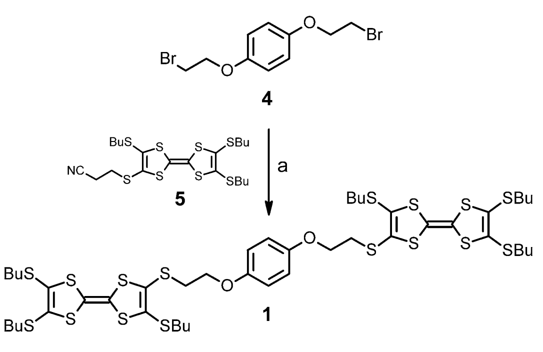

Scheme 1. The synthesis of the TTF monomer **1**: a) **5** (2.0 equiv), CsOH (2.3 equiv), DMF/methanol (10:1), RT, 0.5 h, then **4**, RT, 12 h (29 %).

The general strategy for the synthesis of dimer **2** (and trimer **3**, see below) was first to prepare fully TTF-functionalised phenylene building blocks and then to combine these blocks by means of the Sonogashira coupling methodology (Scheme 2). The iodination of **4** with one equivalent of I_2 led to the monoiodide **6**, which was isolated as a major product along with the known diiodide **7**.[24a] Satisfactorily, compounds **6** and **7** could easily be separated by column chromatography. Compound **6** was fused with two TTF units to afford a functionalised building block **8**. The Sonogashira coupling between **8** and (triisopropylsilyl)acetylene under Pd^0/Cu^I catalysis smoothly provided the ethynylated product **9**, which was desilylated by treatment with tetrabutylammonium fluoride. The resulting alkyne **10** was coupled with iodide **8** under Pd^0/Cu^I catalysis to give rise to the desired dimer **2** in a moderate yield.

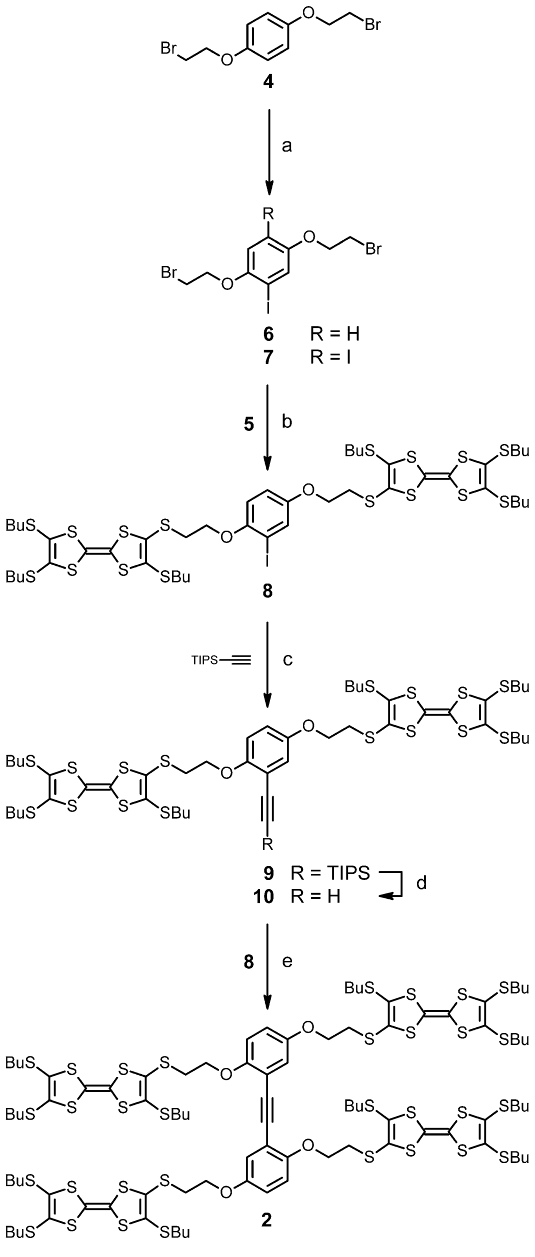

Scheme 2. The synthesis of the TTF dimer **2**: a) I_2 (1.0 equiv), KIO_3 (1.0 equiv), acetic acid, 75 °C, 3 h, 70 % of **6** (23 % of **7**); b) **5** (2.1 equiv), CsOH (2.3 equiv), DMF/methanol (10:1), RT, 0.5 h, then **6**, RT, 3 h (79 %); c) TIPS−C≡CH (2.0 equiv), $[Pd(PPh_3)_4]$ (5 mol %), CuI (15 mol %), diisopropylamine/DMF (1:1), 50 °C, 4 h (92 %); d) $n\mathrm{Bu_4NF}$ (1.1 equiv), THF, RT, 0.5 h (97 %); e) $[Pd(PPh_3)_4]$ (15 mol %), CuI (40 mol %), diisopropylamine/DMF (1:1), 40 °C, 3 h (32 %). TIPS = triisopropylsilyl.

The synthesis of the *p*OPE backbone, such as in trimer **3**, which bears six TTF units, could start either from the central phenylene precursor **11** (to grow simultaneously in two directions) or from the terminal precursor **10** (to grow only in one direction; Scheme 3). Although the former approach allowed the preparation of trimer **3** in moderate yield, the necessity of repeated column-chromatography purification to separate it from numerous minor byproducts disqualified this synthetic pathway. Satisfactorily, the latter approach avoided an arduous purification of the final product. Therefore, we converted the known diiodide **7**[24a] into the symmetrical bis-TTF derivative **11**. Subsequently, we treated **11** with nearly equimolar amount of (triisopropylsilyl)acetylene under Pd^0/Cu^I catalysis to obtain a 3:2 mixture of **12** and **13** along with the minor unreacted diodide **11**. The desired monoethynylated product **12** was easily isolated by column chromatography in a reasonable 45 % yield. The Sonogashira coupling of **10** with **12** led to dimer **14**, which was desilylated with tetrabutylammonium fluoride to afford the terminal alkyne **15**. Finally, cross-coupling of **15** with iodide **8** provided trimer **3** as a clean product in an acceptable yield.

NMR spectroscopic characterisation of the TTF–*p*OPE conjugates: All of the prepared compounds were fully characterised by NMR spectroscopic analysis by means of standard ^1H, ^{13}C, H,H-COSY, H,C-HSQC, and H,C-HMBC techniques (complete signal assignment is given in the Supporting Information). Occasionally, we could see line broadening of the signals in the ^1H NMR spectra for selected TTF derivatives, such as **1** and **14**, even if the measurements were performed in acid-free $CDCl_3$ (to prevent TTF protonation).[40] By changing this solvent to CD_2Cl_2 with similar solvation properties, sharp lines in the ^1H NMR spectra resulted.

Computational study of the TTF–*p*OPE conjugates: To shed light on the molecular shape of the multiple TTF–*p*OPE conjugates **1**–**3**, we studied these molecular structures theoretically. Because of the system size and computer limitations, we used the AM1 semiempirical method for geometry optimisation and the Universal Force Field (UFF) for molecular-dynamics simulations. We focused on the prototypal TTF dimer **2**, the structure of which was first optimised at the AM1 level. Molecular dynamics (MD) were simulated by our in-house program TINK to explore the conformational space. The simulation ran for 1500 ps, and the starting and final geometries of the dimer system **2** are shown in Figure 2. As expected, the molecule exhibited significant conformational freedom to adopt numerous low-lying conformations in the course of the simulation (only one of the

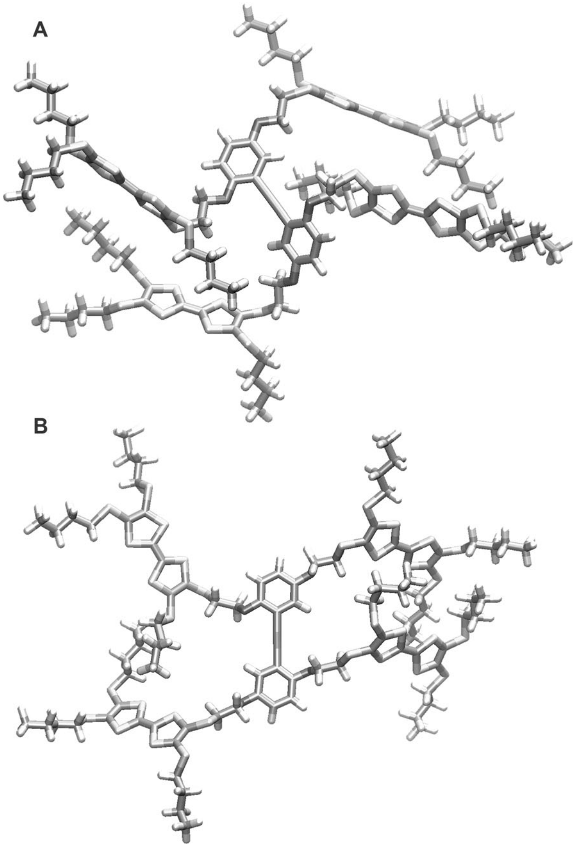

Figure 2. The molecular structure of the TTF dimer **2** obtained by a) AM1 optimisation and B) MD simulation (only one low-lying conformer shown).

populated conformations is shown). Furthermore, MD simulations were performed to scan the conformational space of the TTF monomer **1** to inspect the flexibility necessary to reach a close-to-parallel position of the tethered TTF units (distance: <4 Å). Both the relaxed conformer of **1** and the conformer with intramolecularly stacked TTF units, which were formed during the MD simulation, were treated at the AM1 and B3LYP/6-31G* levels of theory in vacuum to see an energy difference of about 3 kcal mol^{-1} in favour of the relaxed conformer of **1** (see the Supporting Information for further details).

Electrochemical analysis of the TTF–*p*OPE conjugates: The electrochemical experiments were carried out to identify possible communication between the TTF multiple redox centres laterally attached to the *p*OPE backbone. The TTF–

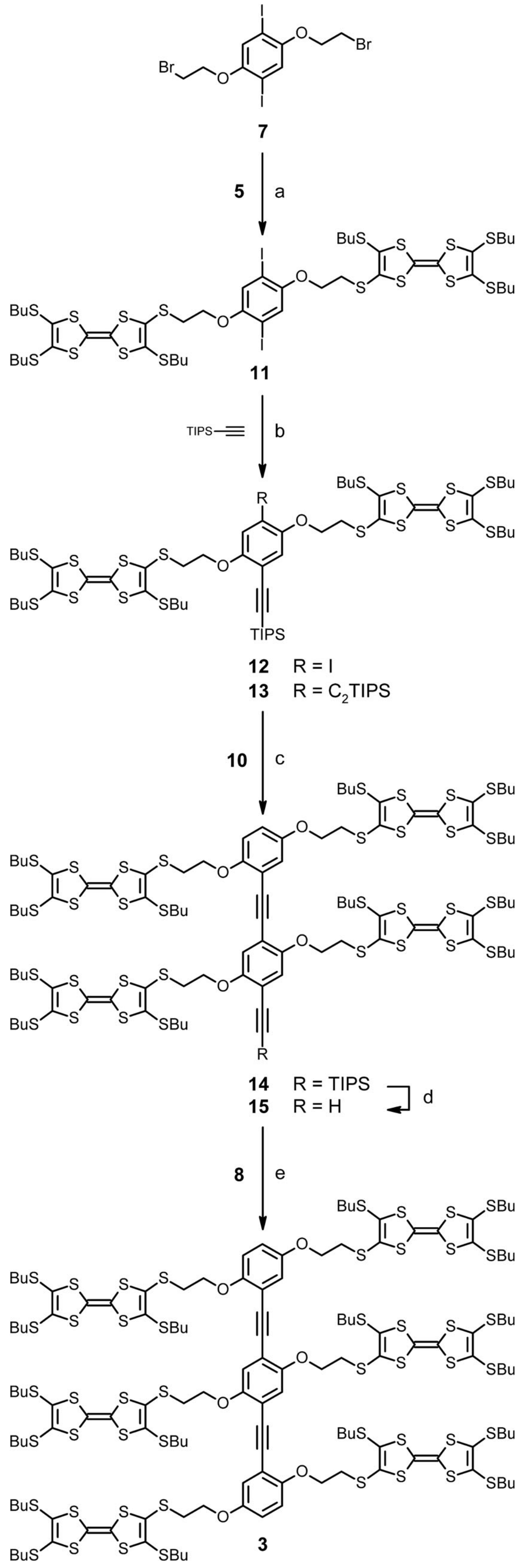

Scheme 3. The synthesis of the TTF trimer **3**: a) **5** (2.1 equiv), CsOH (2.3 equiv), DMF/methanol (10:1), RT, 0.5 h, then **7**, RT, 3 h (70 %); b) TIPS−C≡CH (1.1 equiv), [Pd(PPh$_3$)$_4$] (5 mol %), CuI (15 mol %), diisopropylamine/DMF (1:1), 50 °C, 4 h (45, 30, and 21 % of **12**, **13**, and recovered **11**); c) **10** (1.0 equiv), **12** (1.0 equiv), [Pd(PPh$_3$)$_4$] (15 mol %), CuI (40 mol %), THF/diisopropylamine/DMF (1:1:1), RT, 3 days (45 %); d) nBu$_4$NF (1.1 equiv), THF, RT, 0.5 h (98 %); e) **8** (1.5 equiv), [Pd(PPh$_3$)$_4$] (15 mol %), CuI (40 mol %), THF/diisopropylamine/DMF (1:1:1), 20 °C, 3 days (45 %).

*p*OPE conjugates **1**–**3** were investigated by cyclic voltammetry (CV) at various scan rates (0.05–50 V s^{-1}) by using chronoamperometry and exhaustive electrolysis at two different potentials, which corresponded to the first and second oxidation steps. The cyclic voltammetry of the monomer **1** with two TTF units showed two simple one-electron oxidation steps at 0.489 and 0.853 V (Figure 3). The anodic/cathodic peak separations were 60 mV for both of the redox steps. The other two oligomers **2** and **3** were oxidised practically at the same potentials (Table 1). The anodic/cathodic peak current ratio equalled unity for both the redox steps, and all the TTF–*p*OPE conjugates thus confirmed a reversible electron exchange. The heterogeneous standard rate constant was very high and outside of the measurement limit. The impedance spectroscopy yielded no sign of kinetic control until a frequency as high as 5 kHz. We did not observe any peak splitting for **1**. In contrast, dimer **2** with four TTF units yielded a voltammogram, in which the first oxidation peak seemed to be preceded by a small shoulder. Trimer **3** with six TTF units showed a similar peak overlap for the first oxidation step. The presence of such a small overlapped wave was clearly indicated by the semi-integration followed by the log-plot analysis (see below).

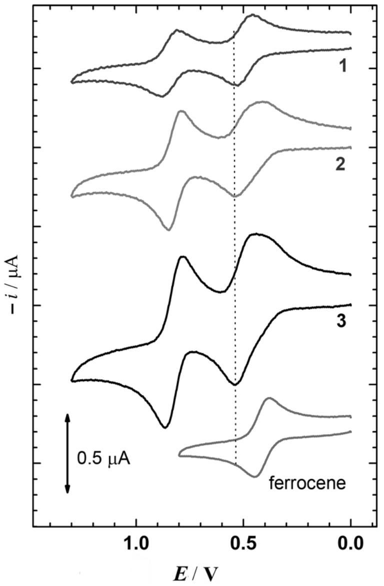

Figure 3. The cyclic voltammetry of 0.2 mM solutions of **1**–**3** and ferrocene (in 0.1 M tetrabutylammonium hexafluorophosphate in dichloroethane at the scan rate of 0.5 V s^{-1}).

Table 1. The formal redox potentials and limiting wave heights of the TTF–*p*OPE conjugates **1**–**3** obtained from the semiintegrated cyclic voltammetry.[a]

Compound	E^0_1 [V]	E^0_2 [V]	$m(\text{lim})_1$ [μC s$^{-1/2}$]	$m(\text{lim})_2$ [μC s$^{-1/2}$]
1	0.489	0.853	0.103	0.096
2	0.482	0.826	0.173	0.176
3	0.488	0.840	0.279	0.276
ferrocene	0.412	–	0.119	

[a] CV in 0.1 M tetrabutylammonium hexafluorophosphate in dichloroethane at the scan rate of 0.5 V s^{-1} referenced to Ag|AgCl|1 M LiCl.

The analysis of the cyclic voltammograms of compounds **1**–**3** under the given conditions indicated that, to our surprise, the charge transferred did not correspond to the number of the TTF units attached. This finding could be inferred from the comparison of the heights of the corresponding peak currents (or the heights of "neo-polarograms", see below) with the height of the peak current of ferrocene at the same molar concentration (Figure 3). Such a controversial observation deserved a detailed study. The analysis of the voltammograms was substantially facilitated by the convolution methods, which transformed current–voltage curves to diagrams identical to those obtained by the steady-state techniques (polarography or rotating disc voltammetry). Voltammograms transformed by semi-integration to "neo-polarograms" (i.e., $m(t)$ vs E)[41] showed the wave/height ratios of 1:1, 2:1, and 3:1 for **1**–**3**, respectively (Figure 4A), which reflected an increased number of the oxidisable units in a molecule. The potential dependence of $\log[m(t)/(m_{\text{lim}}-m(t))]$ for the TTF–*p*OPE conjugates **1**–**3** yielded the log–plot curves with the slope of 59 mV decade^{-1} (Figure 4B, dashed lines), which was characteristic for a one-electron heterogeneous redox step. Hence, the wave/height ratio in Figure 4A just reflected an increased amount of the oxidisable functions present in **1**–**3**. Therefore, the TTF redox centres did not substantially electronically communicate between themselves. Obviously, we observed only

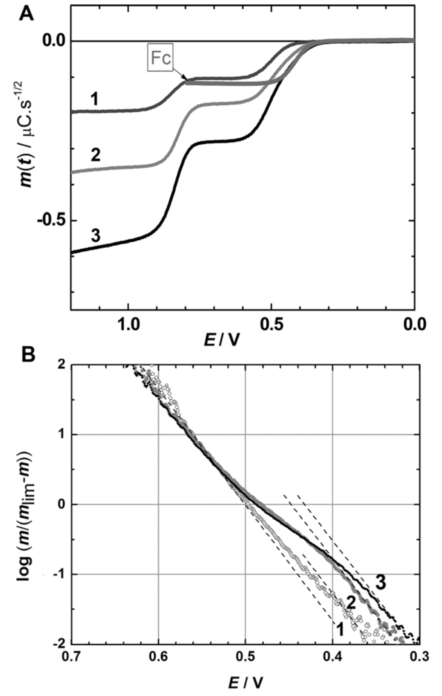

Figure 4. Semiintegration of the positive scans of the voltammograms of **1**–**3** from Figure 3; the wave of ferrocene is labelled as Fc (A). The logarithmic analysis of the first oxidation wave of the semiintegrated voltammograms of **1**–**3** from Figure 3A.

around one half of the electrons transferred relative to that expected. The numerical logarithmic analysis also distinguished the contribution of the small overlapped shoulders present in the first oxidation step of **2** and **3**. Small prepeaks amounted to only few percent of the total current and their position was shifted towards lower potentials by approximately 20, 47, and 60 mV for **1**–**3**, respectively (Figure 4B).

For the sake of indisputably determining the number of electrons n involved in the first oxidation step, we applied two additional independent approaches: the method developed by Malachesky[42] and an exhaustive bulk electrolysis. It is worth noting that the procedure by Malachesky does not require any knowledge of the diffusion coefficient. It yields n from the relationship between the scan-rate dependence of voltammetric peak currents i_p and the time decay of a chronoamperometric transient $i(t)$ measured under diffusion control. Both sets of data have to be measured for the same bulk concentration, the same electrode area, and within a similar timescale. The estimation of n according to the method of Malachesky yielded $n = 1.0 \pm 0.1$, 1.9 ± 0.3, and ≈ 2.5 for **1**–**3**, respectively (Table 2). These values were further confirmed by measuring the faradaic charge consumed during the exhaustive electrolysis at a potential of the diffusion-limited first oxidation (0.75 V). Thus, we could conclude that, in the first redox step, formally only one half of the TTF units of **1**–**3** were oxidised.

Table 2. The number of electrons n per molecule transferred in the first-step electrochemical oxidation of **1**–**3**.[a]

Compound	Expected[b]	Method of Malachesky	Exhaustive electrolysis
1	2	1.0 ± 0.1	1.1 ± 0.05
2	4	1.9 ± 0.3	2.3 ± 0.05
3	6	≈ 2.5	> 2.5

[a] The first oxidation step at 0.75 V. [b] The number of the TTF units per molecule.

The next question to be answered was to estimate the exact number of electrons n transferred in the second oxidation step. The comparable height of the first and second redox peaks in the cyclic voltammograms or neo-polarograms (Figure 4) of **1**–**3** implied that again not all the TTF units were oxidised on the timescale of this process, even at the higher potential (> 1 V) than the respective second oxidation potential (0.8 V; Table 1). The estimation of n in the second oxidation step was verified again by several independent standard electrochemical methods, and the obtained values are consistent. However, the exhaustive bulk electrolysis of **2** at 1 V indeed consumes a charge that corresponds to its oxidation by the total number of eight electrons, as expected from the number of TTF functions in **2**. Compound **3** was electrolyzed at the potential of the second oxidation step and also yielded a charge that corresponds to uptake of twelve electrons, as expected from the presence of six electroactive groups. Although the electrochemical oxidation of **2** and **3** was very slow (within 2 h), the total charge needed to complete the reaction corresponded convincingly to the number of TTF units. Such a slow rate of electrolysis suggests a possible presence of a chemical equilibrium between redox-inactive and redox-active forms.

It is worth noting that electrochemistry of the TTF derivative **5** and 1,4-dibutoxybenzene, which represent simplified models of the key structural elements of **1**–**3**, did not exhibit irregular behaviour of the multiple TTF derivatives mentioned above or did not interfere with the redox-active groups, respectively. The backbone element 1,4-dibutoxybenzene was electrochemically active at potentials at least 0.53 V more positive than the highest oxidation potential of all the TTF derivatives (see the Supporting Information for cyclic voltammograms). The TTF compound **5** could reversibly be oxidised in two steps that represent two one-electron processes, as could be seen from logarithmic analysis of the neo-polarogram obtained by the semi-integration of the cyclic voltammetry curve (see the Supporting Information for further details). The first-step oxidation of **5** was accompanied by the appearance of a NIR band at $\lambda = 2100$ nm. Later, we will show that the half-oxidised **1** yields a similar NIR band shifted by 150 nm towards longer wavelengths.

Such an anomalous behaviour of the TTF–*p*OPE conjugates **1**–**3** in the electrochemical oxidation requires an explanation. The determination of the number of electrons transferred n under given experimental conditions undoubtedly indicates that in the first oxidation step at around 0.5 V formally only one half of the TTF units undergoes a single-electron transfer to form the corresponding $TTF^{+\bullet}$-type radical ion such as $\mathbf{1}^{+\bullet}$ (Scheme 4) or multiple radical cations derived from **2** or **3**. An adequate number of the native TTF units can form mixed-valence D–A complexes with the $TTF^{+\bullet}$ radical ion units in the same molecule (such as in **A**) or different one (such as in **B**–**D**). Furthermore, the radical–

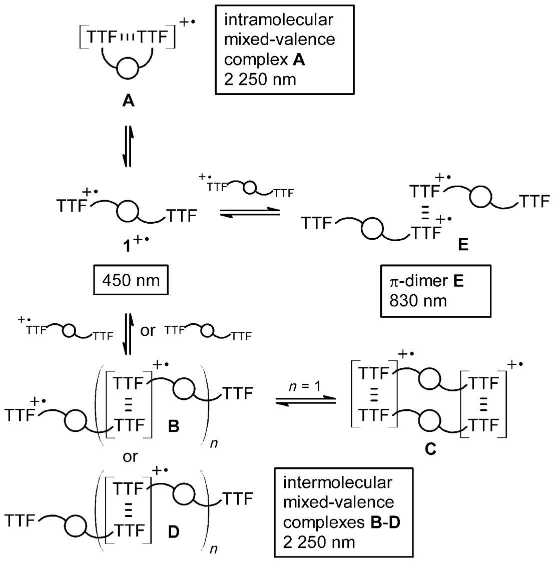

Scheme 4. The possible intra- and intermolecular mixed-valence complexes **A**–**D** and π-dimer **E** formed from the half-oxidised $\mathbf{1}^{+\bullet}$ during the first oxidation step (the characteristic wavelengths of the absorption bands associated with the corresponding forms of the TTF unit(s) are indicated).

radical coupling that results in the formation of a π dimer, such as **E**, is known to participate in the electrochemistry of TTF derivatives.[45b,e,h] Thus, the process that leads to the mixed-valence complexes **A**–**D** must practically be instantaneous and much faster than the first-step oxidation of the TTF units (a complete conversion TTF→$TTF^{+\bullet}$ would otherwise occur).

The mixed-valence complexes in question seem to be oxidatively stable up to the potential of 0.8 V. Obviously, the second-step preparative-scale exhaustive oxidation of all the TTF functions is an overall slow process, regardless of the fact that the electron-transfer rate is very high. It is obvious that a slow homogeneous equilibrium accounts for a long reaction period of the exhaustive bulk electrolysis and, on the other hand, for a smaller height of the peaks of the second oxidation step (at 0.8 V) in the cyclic voltammetry of **1**–**3**, which corresponds also to one half of the expected height. It is worth noting that in this specific case the time scales of the CV and exhaustive electrolysis differ by about the 2–4 orders of magnitude. However, the mixed-valence complexes, such as **A**–**D**, which are rather resistant to oxidation below 0.8 V, might be further slowly oxidised above 0.8 V to the $\mathbf{1}^{4+}$ ion most likely after their slow dissociation back to the $\mathbf{1}^{+\bullet}$ radical ion. Such an equilibrium is absent during the first oxidation step, since the UV/Vis spectra of the solution in situ held after exhaustive electrolysis at the constant potential of the first oxidation step did not change, even after 2 hours at the applied potential. The UV/Vis spectrum did not show any signal that corresponds to the original compound that should be there after hypothetical dissociation of the mixed-valence complex to cation radical and original reactant and the integrated charge was still equal to one. Therefore, a reason for such an unusual behaviour must be sought elsewhere. One possible suggestion is that the silent TTF units are indeed blocked in such a complex and behave differently once the nonsilent TTF units within this complex are oxidised in the second oxidation step. Assuming that the equilibrium is shifted completely towards the mixed valence complex formation (no observation of any UV/Vis signal from the reactant), only the withdrawal of the second electron from the nonsilent TTF unit leads to the availability of the originally electrochemically silent TTF units in the molecule. Therefore, on the time scale of the cyclic voltammetric measurements, only one half of the TTF units is oxidized. We propose that the mixed-valence complex should be formed concomitantly with the first electron-transfer step.

The proposed mechanism of oxidation of the TTF–*p*OPE conjugates **1**–**3** was further supported by spectroelectrochemical data for the characteristic changes in the UV/Vis spectra, which were monitored during the exhaustive electrolysis of **1** and **2** (see Figure 5 for the UV/Vis spectroelectrochemistry of **2**). Upon setting the first-step oxidation potential to 0.6 V, the original UV/Vis maxima at $\lambda = 310$ and 330 nm gradually decreased while two new absorption bands at $\lambda = 450$ and 830 nm appeared (Figure 5 A).

The occurrence of the latter spectral bands is known to reflect the formation of the $TTF^{+\bullet}$-type species[34,35,36c,d,37,43] (Scheme 4). The positions of the absorption maxima observed were in accord with reported data related to the tetrathio-substituted $TTF^{+\bullet}$ radical ions.[33,36c,44] Furthermore, the second-step oxidation at 1 V led to the gradual disappearance of the UV/Vis maxima at $\lambda = 450$ and 830 nm. At the same time, a new strongly absorbing band appeared that gradually shifted its position from $\lambda = 775$ to 722 nm (Figure 5 B). The presence of such a band indicated oxidation of the originally neutral TTF units in **2** to TTF^{2+} units as reported previously (the strong absorption at around $\lambda = 550$–750 nm is characteristic for the TTF^{2+} species).[36c,37,45e]

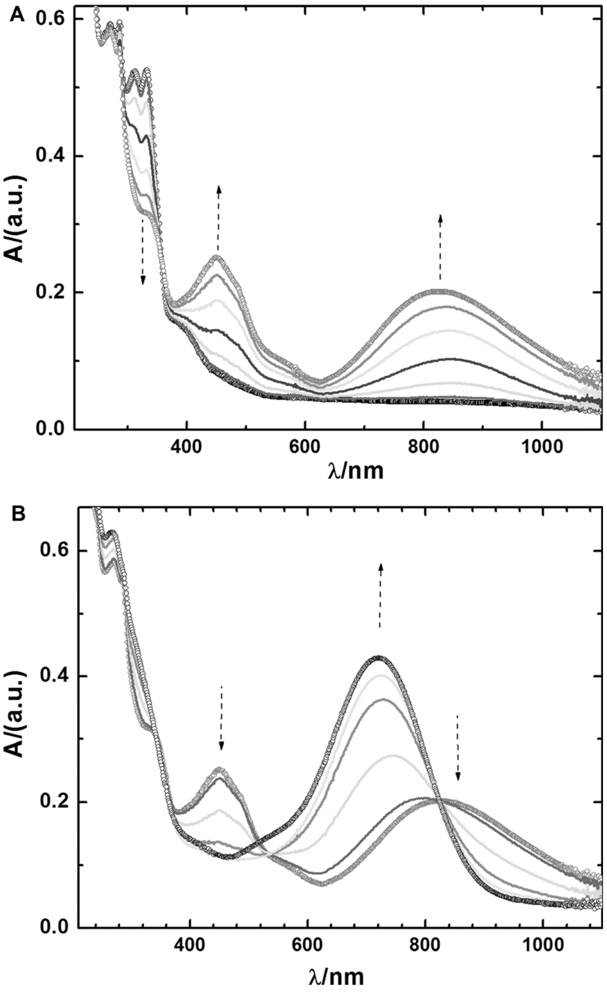

Figure 5. The UV/Vis spectroelectrochemistry of 0.48 mM **2** and 0.2 M tetrabutylammonium hexafluorophosphate in dichloroethane during the electrolysis at A) the first-step redox potential of 0.6 V and B) the subsequent electrolysis at the second-step redox potential of 1.0 V.

We performed an spectroelectrochemical study of **1** in situ in the NIR region at the potential of the first oxidation process (Figure 6) to monitor the formation of the proposed intermediate mixed-valence $[(TTF)_2]^{+\bullet}$-type complexes. A gradual increase of the broad NIR band at $\lambda = 2250$ nm indicated the formation of the aforementioned mixed-valence complex, as it was described for related TTF species ($\lambda =$ 1630–2300 nm).[32,34,35b,36a,b,37,45b,e] It is worth noting that during the electrolysis of **1** at 0.65 V in a thin optical cell

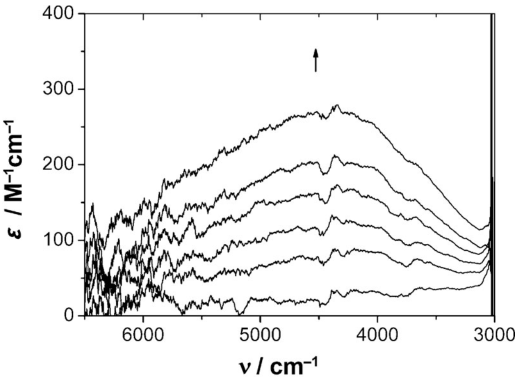

Figure 6. The temporary increase of the NIR absorption band (at $\lambda = 2250$ nm) associated with the proposed formation of a mixed-valence $[(TTF)_2]^{+\bullet}$-type complex during the first-step oxidation of **1** at the potential of 0.6 V (12.3 mM **1**, 0.1 M tetrabutylammonium hexafluorophosphate in dichloroethane).

this band reached its maximum and later gradually disappeared. This behaviour explains why the NIR band can escape the observation if the NIR spectrum is taken ex situ in an exhaustively oxidised sample at the same potential.

The first-step oxidation of **1**–**3** generates the $TTF^{+\bullet}$-type radical ions, which should be paramagnetic (along with their mixed-valence complexes) or diamagnetic if they undergo the radical dimerisation with the formation of a σ bond.[34] Electron spin resonance (ESR) spectroscopy confirmed that the first-step oxidation of these compounds at 0.7 V led to a radical species because the ESR signal was observed (see Figure 7 for the ESR spectrum of oxidized species **2**). The temperature-dependent measurements showed that whereas a single-line spectrum was observed at 20 °C, fine splitting of the signal appeared at −63 °C. We propose that this behaviour stems from a dynamic equilibrium between inter- and intramolecular complexes or their conformers, which proceeds quickly on the ESR timescale at ambient temperature or is frozen at a low temperature.

The observation that upon the first-step oxidation at 0.5 V formally one half of the TTF units in **1**–**3** remain, surprisingly, electrochemically silent is not in accord with the earlier studies on the intramolecular mixed-valence $[(TTF)_2]^{+\bullet}$-type complexes. If the two communicating TTF redox centres generate a mixed-valence complex during the first-step oxidation, then, usually, a broadening or splitting of the corresponding CV wave appears.[36c,45] This finding is generally explained by facilitating the first single-electron transfer because the formation of a $[(TTF)_2]^{+\bullet}$-type dyad stabilises a $TTF^{+\bullet}$-type intermediate. This outcome results in hampering the second single-electron transfer (due to the electrostatic repulsion in a $[(TTF)_2]^{2+}$-type intermediate).[45g] However, there is seemingly no substantial splitting of the first-step oxidation wave in the case of **1**.

The fact that formally one half of the TTF units are electrochemically silent at the first-step oxidation potential means that either one half of the TTF units in all the molecules or all the TTF units in one half of the molecules are oxidised to the $TTF^{+\bullet}$ state (if we consider two limiting situations). The latter case invokes a hypothesis that the oxidation is incomplete but the number of electrons transferred in the oxidised molecules is twofold greater than observed (see Table 2 for the oxidation of **1**–**3**). As for **1**, the measured first one-electron oxidation at 0.7 V might involve a hidden two-electron process, for which a suggested reaction mechanism $\mathbf{1} \rightarrow \mathbf{1}^{+\bullet} \rightarrow \mathbf{1}^{2+2\bullet}$ is given in Scheme 5 (possible oligomeric mixed-valence complexes were omitted). Its numerical simulation using the finite difference methods[50] showed that at large values of the rate constant k_2 the original two-electron wave changes to a single-electron wave (Figure 8). Hence, the first oxidation step involves a stepwise oxidation of both TTF units in some molecules **1**, which is accompanied by the very fast formation of the mixed-valence complexes **D** and **C**. The rate of the formation of **D** is less important and gives rise to a small shoulder seen on the log–plot diagrams (see the Supporting Information). The rate constant for the formation of **C** is at least $k_2 \geq 10^4\,\text{M}^{-1}\text{s}^{-1}$ (the simulations are not sensitive to a large k_2 value and hence a more accurate estimate is not available). We are aware that Scheme 5 omits the formation of π dimers, for which absorption at $\lambda = 830$ nm was observed and considered in Scheme 4. However, the formation of these dimers

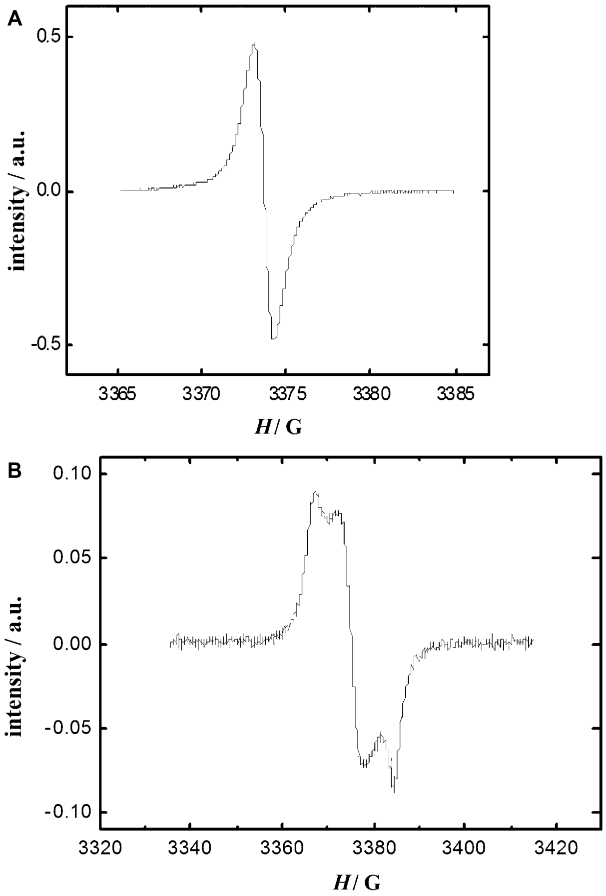

Figure 7. The ESR spectrum at A) 20 and B) −63 °C of **2** oxidised at 0.7 V in dichloroethane.

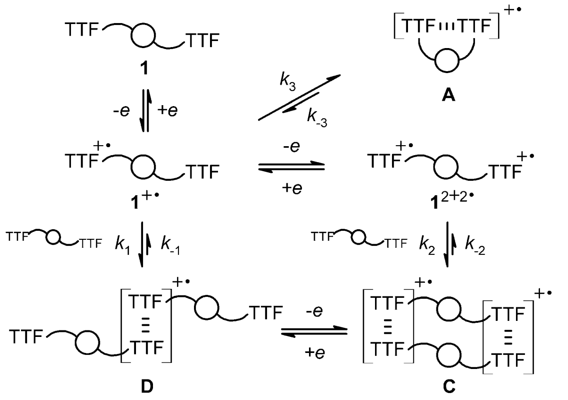

Scheme 5. The proposed mechanism of the oxidation of **1** in the first oxidation step at 0.5 V. Numerical simulation shows that $k_2 > 1000$ leads to a formal one-electron voltammetric currents.

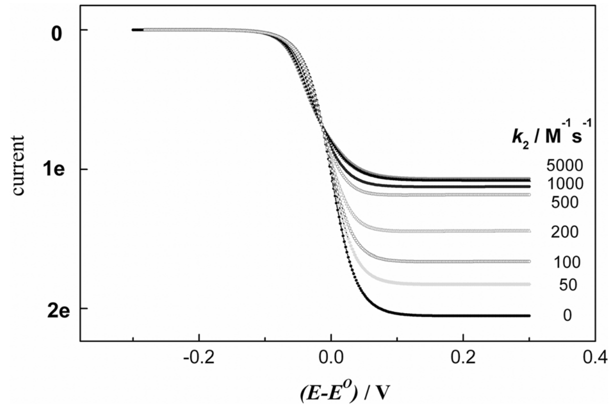

Figure 8. The numerical simulation of the steady state current-voltage dependence for the mechanism given in Scheme 5. Standard heterogeneous rate constants were assumed to be high (1 cm s^{-1}) and other kinetic constants were $k_1 = k_3 = k_{-1} = k_{-2} = 0$.

does not lead to the consumption of the starting material **1** and, therefore, cannot explain the one-electron character of the waves.

To provide a rationale why formally one half of the TTF units contained in solutions of **1**–**3** remains electrochemically silent upon the first-step oxidation at 0.5 V, we suggest the formation of mixed-valence complexes exemplified by **A**–**D**, as discussed above (Schemes 4 and 5). Two scenarios might be proposed to explain why all the TTF units in the mixed-valence complexes are not converted into the TTF$^{+\bullet}$ state at the first-step oxidation potential: 1) The mixed-valence complexes derived from **1**–**3** are unusually resistant to the further oxidation until the oxidation potential of 0.8 V is achieved. This behaviour suggests that below this potential the oxidation of the respective mixed-valence complexes is extremely slow (kinetically controlled). A large shift of redox potentials upon complexation of metallic cations has been well known for decades. 2) Alternatively, by forming mixed-valence complexes, the first-step oxidation wave is split to such an extent (ca. $\lambda = 350$ mV) that its higher-potential part overlaps with the second-step oxidation wave (thermodynamically controlled). However, the first and second oxidation wave in the cyclic voltammograms of **1**–**3** should be in a 1:3 ratio but not of the approximately same height as we observed (Figure 3).[51] Accordingly, the suggested explanation based on the astounding kinetic stability of the $[(TTF)_2]^{+\bullet}$-type mixed-valence complexes at 0.5 V and their slow oxidation to the TTF^{2+}-type state above 0.8 V seems to be more probable.

Conclusions

We have synthesised the new TTF–*p*OPE conjugates **1**–**3**, which resemble short double-sided combs bearing two, four, or six electroactive TTF groups laterally attached to the central phenylene unit or *p*OPE rod. The syntheses of dimer **2** and trimer **3** have been based on the Sonogashira coupling between the TTF-functionalised aryl iodides and aryl acetylenes. Compounds **1**–**3** were characterised in detail by NMR spectroscopic analysis, and the lowest-energy conformers of these compounds were identified by using DFT computational methods.

Intriguingly, the electrochemical oxidation of the TTF–*p*OPE conjugates **1**–**3** provided unexpected results. Despite the fact that the TTF derivatives are usually oxidised in two consecutive waves to generate first the TTF$^{+\bullet}$-type radical ion, which is converted into the TTF^{2+}-type ion at higher redox potentials, we surprisingly found one half of the TTF units in solutions of **1**–**3** to be seemingly electrochemically silent during the first-step oxidation. The kinetic simulations and the presence of the NIR mixed-valence band at $\lambda = 2250$ nm indicated that the first-step oxidation (at 0.5 V) of the prototypal **1** bearing two TTF units might be a hidden two-electron process, in which the doubly oxidised molecules $\mathbf{1}^{2+2\bullet}$ interacted with the nonoxidised species **1** to form the persistent mixed-valence complexes of the TTF–TTF$^{+\bullet}$ type. The experimental data obtained from cyclic voltammetry, exhaustive bulk electrolysis, spectroelectrochemistry, UV/Vis–NIR, and ESR spectroscopy were consistent with this observation. Such complexes exhibited a remarkable kinetic stability towards oxidation, which, consequently, hindered the oxidation of all the TTF units to the TTF$^{+\bullet}$ radical ions at the first-step oxidation potential.

These results provide new stimuli for further research activities focused on the structure of multiple mixed-valence (or D–A) complexes derived from the TTF–*p*OPE conjugates, on the formation of the intramolecular π-delocalised stacks of the $[(TTF)_2]^{+\bullet}$ dyads, on a possible role of the π-conjugated *p*OPE backbone in electron-transfer processes and, last but not least, on designing the proper partners to control their zipping driven by a multiple intermolecular D–A interactions.

Experimental Section

Computational details: Gaussian09 package[46] was used to perform the AM1 semiempirical calculations. Constant-energy molecular-dynamics simulations were run with our in-house program TINK[47] and the UFF[48] force field. The simulation time step was 1 fs; the initial temperature was 300 K. Charges were assigned by the charge equilibration scheme.[49]

Electrochemistry, spectroelectrochemistry, and ESR spectroscopy: Electrochemical measurements were performed using a potentiostat/galvanostat Autolab PGSTAT30 equipped with a frequency response module (Eco Chemie, The Netherlands). A three-electrode electrochemical cell was used. The reference electrode, Ag|AgCl|1 M LiCl, was separated from the test solution by a nonaqueous salt bridge. The potential of the ferrocene/ferrocenium redox couple (Fc/Fc^+) was 0.412 V. The working electrode was a glass-sealed Au disc 0.5 mm in diameter. The auxiliary electrode was a platinum wire. The scan rate of the applied DC potential was in the range 0.05–50 $V\,s^{-1}$. Tetrabutylammonium hexafluorophosphate ($TBAPF_6$) and dichloroethane were supplied by Sigma Aldrich. The indifferent electrolyte $TBAPF_6$ was recrystallised and dried under vacuum. Dichloroethane was dried over activated molecular sieves. Oxygen was removed from the solution by passing a stream of argon saturated with vapours of the solvent. The spectroelectrochemical data were obtained in an optically transparent thin-layer cell. The spectra were recorded using a diode-array UV/Vis spectrometer from Hewlett–Packard (model 8452A) and a UV/Vis–NIR spectrometer from PerkinElmer (Lambda 1050 model). The solutions of the cation radicals for the ESR spectroscopic analysis were prepared by an exhaustive electrolysis in a cell with a separated compartment of the counterelectrode and transferred under inert atmosphere to a flat quartz cuvette. The ESR spectra were measured with a Bruker ELEKSYS E-500 spectrometer. The modulation frequency was 100 kHz. The modulation amplitude was 0.05–0.1 G. Voltammograms (the dependence of the current i on the applied potential E) were numerically transformed to semi-integrated "neopolarograms", which give the dependence of a semi-integral $m(t)$ as a function of the applied potential E in the form of a sigmoid wave with a limiting height of m_{lim}.

Materials and procedures: The melting points were determined on a Kofler hot-stage apparatus and are uncorrected. The ^1H NMR spectra were measured at 400.13, 499.88, and 600.13 MHz, the ^{13}C NMR spectra at 100.61, 125.71, and 150.90 MHz in $CDCl_3$ with TMS as an internal standard or CD_2Cl_2. The chemical shifts are given in δ and the coupling constants J are given in Hz. The HMBC experiments were set up for $J_{C-H}=5$ Hz. For correct assignment of both the ^1H and ^{13}C NMR spectra of key compounds, COSY, HMQC, and HMBC experiments were performed. The IR spectra were measured in CCl_4. The EI mass spectra were determined at an ionising voltage of 70 eV, the m/z values are given along with their relative intensities (%). The standard spectra measured with 70 eV were recorded in the positive ion mode. The TOF EI spectra were measured by using an orthogonal acceleration time-of-flight mass spectrometer GCT Premier (Waters). The sample was dissolved in chloroform, loaded into a quartz cup of the direct probe, and inserted into the ion source. The source temperature was 220 °C. For exact mass measurement, the spectra were internally calibrated using perfluorotri-n-butylamine (Heptacosa). The ESI mass spectra were recorded using the LCQ classic ion-trap mass spectrometer (Thermo) equipped with an electrospray ion source and controlled by Xcalibur software. The mobile phase consisted of methanol/water (9:1) with a flow rate of 200 $\mu L\,min^{-1}$. The samples were dissolved in chloroform, diluted with the mobile phase, and injected with a 5 µL loop. The exact mass was measured using an LTQ Orbitrap XL hybrid mass spectrometer (Thermo Fisher Scientific; Waltham, MA, USA) equipped with an electrospray ion source. The mobile phase consisted of methanol/water (9:1) with a flow rate of 100 $\mu L\,min^{-1}$. The sample was dissolved in chloroform, diluted with the mobile phase, and injected using a 2 µL loop. The mass spectra were internally calibrated by using the known impurities in the mobile phase. Accurate mass measurements were obtained by EI or ESI mass-spectrometric analysis. Combustion analyses were performed by a PE 2400 Series II CHNS/O Analyzer (Perkin Elmer) with an accuracy of CHN determination better than 0.30 % abs. Commercially available catalysts and reagent-grade materials were used as received. Decane was degassed by three freeze/pump/thaw cycles before use. Diisopropylamine was distilled from calcium hydride under argon; THF was freshly distilled from sodium/benzophenone under nitrogen; DMF was degassed by three freeze/pump/thaw cycles before use, HPLC-grade methanol was stored over molecular sieves. The TLC analysis was performed on silica gel 60 F_{254}-coated aluminium sheets (Merck), and the spots were detected by a solution of $Ce(SO_4)_2{\cdot}4H_2O$ (1 %) and $H_3P(Mo_3O_{10})_4$ (2 %) in sulfuric acid (10 %). The chromatography was performed on silica gel 60 (0.040–0.063 mm; Fluka).

4,4′-[Benzene-1,4-diylbis(oxyethane-2,1-diylsulfanediyl)]bis[4′,5,5′-tris(butylsulfanyl)-2,2′-bi-1,3-dithiole] (1): A Schlenk flask was charged with tetrathiafulvalene **5** (103 mg, 0.186 mmol, 2.0 equiv), flushed with argon, and DMF (7 mL) was added. A solution of $CsOH{\cdot}H_2O$ (36 mg, 0.214 mmol, 2.3 equiv) in methanol (0.5 mL) was slowly added to the reaction mixture, which was stirred at room temperature for 0.5 h. Dibromide **4** (30 mg, 0.093 mmol, 1.0 equiv) dissolved in DMF (3 mL) was added and the reaction mixture was stirred at room temperature for 12 h. The solvent was removed in vacuo, and the crude product was purified by column chromatography on silica gel (hexane/chloroform 70:30) to provide **1** (31 mg, 29 %) as a red amorphous solid. ^1H NMR (500 MHz, CD_2Cl_2): $\delta=0.90$, 0.915, 0.92 (3×t, 18H, $J_{vic}=7.4$ Hz), 1.36–1.48, 1.55–1.65 (2×m, 24H), 2.81, 2.825 (2×t, 12H, $J_{vic}=7.3$ Hz), 3.15 (t, 4H, $J_{vic}=6.5$ Hz), 4.11 (t, 4H, $J_{vic}=6.5$ Hz), 6.83 ppm (s, 4H); ^{13}C NMR (125.7 MHz, CD_2Cl_2): $\delta=13.91$, 13.93, 13.94 (4×q), 22.2 (t), 32.37, 32.38, 32.39 (3×t), 35.7 (t), 36.52, 36.54 (2×t), 68.0 (t), 110.0, 111.6 (2×s), 116.2 (d), 126.2 (s), 128.3, 128.4, 130.9 (3×s), 153.4 ppm (s); IR (CCl_4): $\tilde{\nu}=2961$, 2932, 2875, 2864, 1614, 1593, 1507, 1465, 1380, 1226, 1033 cm^{-1}; UV/Vis ($ClCH_2CH_2Cl$): λ_{max} ($\log\varepsilon$) = 311 (3.01), 332 (3.05), 350 nm (3.03); MS (TOF MALDI): m/z: 1162 [M^+]; MS (ESI+): m/z: 1201 ([M+K]$^+$), 1185 ([M+Na]$^+$), 1162 [M^+]; HRMS (ESI+): m/z calcd for $C_{57}H_{86}O_2S_{16}$: 1162.0584 [M^+]; found: 1162.0589.

4,4′,4″,4‴-{Ethyne-1,2-diylbis[benzene-2,1,4-triylbis(oxyethane-2,1-diylsulfanediyl)]}tetrakis[4′,5,5′-tris(butylsulfanyl)-2,2′-bi-1,3-dithiole] (2): A Schlenk flask was charged with **10** (97.0 mg, 0.082 mmol), $[Pd(PPh_3)_4]$ (14.3 mg, 0.012 mmol, 15 mol %), and CuI (6.2 mg, 0.033 mmol, 40 mol %); flushed with argon; and then a solution of **8** (105.6 mg, 0.082 mmol, 1.0 equiv) in diisopropylamine (8 mL) and DMF (8 mL) was added. The reaction mixture was stirred at 40 °C for 3 h. The solvent was removed in vacuo, and the crude product was purified by column chromatography on silica gel (chloroform/hexane 40:60) to provide **2** (61.0 mg, 32 %) as a red amorphous solid. ^1H NMR (400 MHz, $CDCl_3$, TMS): $\delta=0.897$, 0.904, 0.917, 0.923 (4×t, 36H), 1.35–1.49, 1.54–1.66 (2×m, 48H), 2.82 (t, 24H, $J_{vic}=7.3$ Hz), 3.17 (t, 4H, $J_{vic}=6.5$ Hz), 3.23 (t, 4H, $J_{vic}=6.9$ Hz), 4.14 (t, 4H, $J_{vic}=6.5$ Hz), 4.24 (t, 4H, $J_{vic}=6.9$ Hz), 6.86 (m, 4H), 7.07 ppm (dd, 2H, $J_{6,4}=1.7$ Hz); ^{13}C NMR (100.6 MHz, $CDCl_3$, TMS): $\delta=13.55$, 13.59 (2×q), 21.59, 21.61 (2×t), 31.69, 31.72, 31.74 (3×t), 35.0 (t), 35.90, 35.92 (2×t), 67.4 (t), 68.8 (t), 89.8 (s), 109.25, 109.32, 111.0 (3×s), 114.5 (s), 115.1 (d), 116.6 (d), 119.0 (d), 125.1, 125.2 (2×s), 127.56, 127.57, 127.8, 130.28, 130.34 (5×s), 152.5 (s), 153.4 ppm (s); IR (CCl_4): $\tilde{\nu}=2961$, 2931, 2874, 2863, 2216, 1601, 1577, 1495, 1465, 1380, 1222, 1031 cm^{-1}; UV/Vis ($ClCH_2CH_2Cl$): λ_{max} ($\log\varepsilon$) = 263 (4.77), 313 (4.72), 333 nm (4.75); MS (TOF MALDI): m/z: 2346 [M^+].

4-{[2-(2,5-Bis{[2,5-bis(2-{[4′,5,5′-tris(butylsulfanyl)-2,2′-bi-1,3-dithiol-4-yl]sulfanyl}ethoxy)phenyl]ethynyl}-4-(2-{[4′,5,5′-tris(butylsulfanyl)-2,2′-bi-1,3-dithiol-4-yl]sulfanyl}ethoxy)phenoxy]ethyl}sulfanyl)-4′,5,5′-tris(butylsulfanyl)-2,2′-bi-1,3-dithiole (3): A Schlenk flask was charged with **8** (81.4 mg, 0.063 mmol), $[Pd(PPh_3)_4]$ (11.0 mg, 0.009 mmol, 15 mol %), and CuI (5.0 mg, 0.028 mmol, 40 mol %); flushed with argon; and then solution of **15** (100.0 mg, 0.0421 mmol, 1.5 equiv) in diisopropylamine (5 mL), DMF (5 mL), and THF (5 mL) was added. The reaction mixture was stirred at room temperature for 3 days. The solvent was removed in vacuo, and the crude product was purified by column chromatography on silica gel (chloroform/hexane 40:60) to provide **3** (101.2 mg, 45 %) as a red amorphous solid. ^1H NMR (600 MHz, $CDCl_3$, TMS): $\delta=0.87$–0.94 (m, 54H), 1.35–1.47, 1.55–1.65, 2.79–2.86 (3×m, 108H), 3.17, 3.24, 3.27 (3×t, 12H, $J_{vic}=6.5$ Hz), 4.15, 4.25, 4.28 (3×t, 12H, $J_{vic}=6.5$ Hz), 6.86, 6.87 (2×

m, 4H), 7.089 (s, 2H), 7.090 ppm (dd, 2H, $J_{6',4'}=2.0$, $J_{6',3'}=1.4$ Hz); ^{13}C NMR (150.9 MHz, $CDCl_3$, TMS): $\delta=13.61$, 13.62, 13.63, 13.7 (4×q), 21.6, 21.68, 21.69 (3×t), 31.7, 31.77, 31.80 (3×t), 34.99, 35.04, 35.2 (3×t), 35.95, 35.97 (2×t), 67.4, 68.6 (2×t), 89.9 (s), 91.6 (s), 109.4, 111.1 (2×s), 114.2 (s), 114.7 (s), 114.9 (d), 116.8 (d), 118.2 (d), 119.0 (d), 125.1, 125.3 (2×s), 127.56, 127.63, 127.8, 130.36, 130.40, 130.43 (6×s), 152.5 (s), 153.1 (s), 153.5 ppm (s); IR (CCl_4): $\tilde{\nu}=2961$, 2930, 2874, 2862, 2210, 1602, 1578, 1506, 1493, 1465, 1380, 1216, 1027 cm^{-1}; UV/Vis ($ClCH_2CH_2Cl$): $\lambda_{\max}$ ($\log\varepsilon$)=307 (4.76), 332 (4.72), 350 (4.51), 378 nm (4.47); MS (TOF MALDI): m/z: 3530 [M^+].

1,4-Bis(2-bromoethoxy)-2-iodobenzene (6) and 1,4-bis(2-bromoethoxy)-2,5-diiodobenzene (7): A round flask was charged with dibromide **4** (9.27 g, 28.6 mmol), KIO_3 (6.12 g, 28.6 mmol, 1.0 equiv), iodine (3.63 g, 28.6 mmol, 1.0 equiv) and then acetic acid (300 mL) and conc. H_2SO_4 (3 mL) were added to the reaction mixture, which was stirred at 75 °C for 3 h. After cooling, water (100 mL) was added to the reaction mixture, a saturated solution of Na_2SO_3 was added, and the organic layer was extracted with chloroform (5×200 mL). The organic phases were collected, washed with water (2×50 mL), and dried over $MgSO_4$. The solvent was removed in vacuo, and the crude reaction mixture was purified by column chromatography on silica gel (chloroform/hexane 30:70) to provide monoiodide **6** (8.11 g, 65 %) as a solid and diiodide **7** (4.27 g, 26 %) as a solid. Compound **6**: M.p.: 73–74 °C (hexane); ^{1}H NMR (500 MHz, $CDCl_3$, TMS): $\delta=3.60$ (t, 2H, $J_{\mathrm{vic}}=6.2$ Hz), 3.66 (t, 2H, $J_{\mathrm{vic}}=6.4$ Hz), 4.21 (t, 2H, $J_{\mathrm{vic}}=6.2$ Hz), 4.27 (t, 2H, $J_{\mathrm{vic}}=6.4$ Hz), 6.78 (d, 1H, $J_{3,4}=8.9$ Hz), 6.88 (dd, 1H, $J_{4,3}=8.9$, $J_{4,6}=3.0$ Hz), 7.36 ppm (d, 1H, $J_{6,4}=3.0$ Hz); ^{13}C NMR (125.7 MHz, $CDCl_3$, TMS): $\delta=28.8$ (t), 29.0 (t), 68.7 (t), 70.3 (t), 87.5 (s), 114.3 (d), 115.9 (d), 126.0 (d), 152.0 (s); 153.4 ppm (s); IR (CCl_4): $\tilde{\nu}=2934$, 2862, 1598, 1575, 1487, 1456, 1209, 1017 cm^{-1}; MS (TOF EI+): m/z (%): 452 ([$M^{+\cdot}$] with ^{81}Br^{81}Br, 32), 450 ([$M^{+\cdot}$] with ^{79}Br^{81}Br, 65), 448 ([$M^{+\cdot}$] with ^{79}Br^{79}Br, 33), 343 (33), 341 (34), 235 (8), 135 (8), 109 (95), 107 (100); HRMS (EI+): m/z calcd for $C_{10}H_{11}O_2{}^{79}Br_2I$: 447.8171 [$M^+$]; found: 447.8169. Compound **7**: M.p. 144 °C (hexane), lit. 141–142 °C.[24a]

4,4′-[(2-Iodobenzene-1,4-diyl)bis(oxyethane-2,1-diylsulfanediyl)]-bis[4′,5,5′-tris(butylsulfanyl)-2,2′-bi-1,3-dithiole] (8): A Schlenk flask was charged with tetrathiafulvalene **5** (2.72 g, 4.91 mmol. 2.1 equiv), flushed with argon, and DMF (150 mL) was added. A solution of $CsOH{\cdot}H_2O$ (861 mg, 5.129 mmol, 2.3 equiv) in methanol (15 mL) was slowly added to the reaction mixture, which was stirred at room temperature for 30 min. Dibromide **6** (1.0 g, 2.23 mmol) dissolved in DMF (3 mL) was added to the reaction mixture, which was stirred further at room temperature for 12 h. The solvent was removed in vacuo, and the crude product was purified by column chromatography on silica gel (chloroform/hexane 60:40) to provide iodide **8** (2.26 g, 79 %) as a solid. M.p. 81.0–81.5 °C (hexane); ^{1}H NMR (600 MHz, $CDCl_3$, TMS): $\delta=0.89$, 0.91, 0.921, 0.922, 0.926, 0.930 (6×t, 18H, $J_{\mathrm{vic}}=7.4$ Hz), 1.36–1.48, 1.56–1.65, 2.80–2.84 (3×m, 36H), 3.13 (t, 2H, $J_{\mathrm{vic}}=6.6$ Hz), 3.21 (t, 2H, $J_{\mathrm{vic}}=6.6$ Hz), 4.09 (t, 2H, $J_{\mathrm{vic}}=6.6$ Hz), 4.14 (t, 2H, $J_{\mathrm{vic}}=6.6$ Hz), 6.76 (d, 1H, $J_{3,4}=9.0$ Hz), 6.85 (dd, 1H, $J_{4,3}=9.0$, $J_{4,6}=2.9$ Hz), 7.33 ppm (d, 1H, $J_{6,4}=2.9$ Hz); ^{13}C NMR (150.9 MHz, $CDCl_3$, TMS): $\delta=13.56$, 13.59 (2×q), 21.6 (t), 31.7, 31.8 (2×t), 34.8, 35.8 (2×t), 35.92, 35.94, 36.0 (3×t), 67.4 (t), 69.2 (t), 87.2 (s), 109.2, 109.5, 111.2, 111.3 (4×s), 113.6 (d), 115.6 (d), 124.8, 125.3 (2×s), 125.7 (d), 127.6, 127.76, 127.78, 130.4, 130.8 (5×s), 151.9 (s), 153.3 ppm (s); IR (CCl_4): $\tilde{\nu}=2961$, 2931, 2875, 2864, 1598, 1574, 1478, 1465, 1380, 1212, 1018 cm^{-1}; UV/Vis (CH_3CN): $\lambda_{\max}$ ($\log\varepsilon$)=218 (4.78), 263 (4.34), 308 (4.51), 332 nm (4.31); MS (TOF MALDI): m/z: 1288 [M^+]; MS (TOF ESI+): m/z: 1327 ([M+K]$^+$), 1311 ([M+Na]$^+$), 1288 [M^+]; HRMS (EI+): m/z calcd for $C_{46}H_{65}IO_2S_{16}$: 1287.9563 [M^+]; found: 1287.9555.

{[2,5-Bis(2-{[4′,5,5′-tris(butylsulfanyl)-2,2′-bi-1,3-dithiol-4-yl]sulfanyl}ethoxy)phenyl]ethynyl}[tris(1-methylethyl)]silane (9): A Schlenk flask was charged with **8** (600 mg, 0.466 mmol), [$Pd(PPh_3)_4$] (26.9 mg, 0.023 mmol, 5 mol %), and CuI (12.7 mg, 0.067 mmol, 15 mol %); flushed with argon; and then diisopropylamine (8 mL) and DMF (8 mL) were added. (Triisopropylsilyl)acetylene (0.207 mL, 0.932 mmol, 2.0 equiv) was added dropwise over 30 min to the reaction mixture, which was stirred at 50 °C for 4 h. The solvent was removed in vacuo, and the crude product was purified by column chromatography on silica gel (chloroform/hexane 50:50) to provide **9** (575 mg, 92 %) as a red amorphous solid. ^{1}H NMR (600 MHz, $CDCl_3$, TMS): $\delta=0.90$, 0.91, 0.920, 0.921, 0.924, 0.925 (6×t, 18H, $J_{\mathrm{vic}}=7.4$ Hz), 1.14 (m, 21H), 1.37–1.48, 1.55–1.65, 2.79–2.84 (3×m, 36H), 3.14 (t, 2H, $J_{\mathrm{vic}}=6.6$ Hz), 3.15 (t, 2H, $J_{\mathrm{vic}}=7.0$ Hz), 4.10 (t, 2H, $J_{\mathrm{vic}}=6.6$ Hz), 4.15 (t, 2H, $J_{\mathrm{vic}}=7.0$ Hz), 6.80 (d, 1H, $J_{3,4}=8.9$ Hz), 6.82 (dd, 1H, $J_{4,3}=8.9$, $J_{4,6}=2.9$ Hz), 6.97 ppm (d, 1H, $J_{6,4}=2.9$ Hz); ^{13}C NMR (150.9 MHz, $CDCl_3$, TMS): $\delta=11.3$ (d), 13.6 (q), 18.7 (q), 21.6 (t), 31.7 (t), 34.8 (t), 35.0 (t), 35.9 (t), 67.3 (t), 68.4 (t), 95.5 (s), 102.5 (s), 114.4 (s), 114.5 (d), 116.4 (d), 119.5 (d), 125.2, 125.3 (2×s), 127.6, 127.8, 130.2, 130.5 (4×s), 152.3 (s) 154.2 ppm (s); =CS_2 not detected; IR (CCl_4): $\tilde{\nu}=2961$, 2932, 2875, 2865, 2155, 1603, 1579, 1496, 1465, 1381, 1224, 1031 cm^{-1}; UV/Vis ($ClCH_2CH_2Cl$): $\lambda_{\max}$ ($\log\varepsilon$)=219 (4.79), 262 (4.61), 312 (4.47), 330 nm (4.31); MS (TOF MALDI): m/z: 1342 [M^+]; MS (TOF ESI+): m/z: 1381 ([M+K]$^+$), 1365 ([M+Na]$^+$), 1342 [M^+]; HRMS (ESI+): m/z calcd for $C_{57}H_{86}O_2NaS_{16}Si$: 1365.1799 [($M$+Na)$^+$]; found: 1365.1821.

4,4′-[(2-Ethynylbenzene-1,4-diyl)bis(oxyethane-2,1-diylsulfanediyl)]-bis[4′,5,5′-tris(butylsulfanyl)-2,2′-bi-1,3-dithiole] (10): A Schlenk flask was charged with **9** (560 mg, 0.417 mmol), flushed with argon, and solution of nBu$_4$NF·3H$_2$O (145 mg, 0.459 mmol, 1.1 equiv) in THF (15 mL) was added. The reaction mixture was stirred at room temperature for 30 min. The solvent was removed in vacuo, and the crude product was purified by column chromatography on silica gel (chloroform) to provide **10** (479 mg, 97 %) as a red oil. ^{1}H NMR (500 MHz, $CDCl_3$, TMS): $\delta=0.906$, 0.908, 0.921, 0.922, 0.926, 0.928 (6×t, 18H, $J_{\mathrm{vic}}=7.4$ Hz), 1.37–1.48, 1.56–1.65, 2.80–2.85 (3×m, 36H), 3.14 (t, 2H, $J_{\mathrm{vic}}=6.6$ Hz), 3.19 (t, 2H, $J_{\mathrm{vic}}=7.2$ Hz), 3.27 (s, 1H), 4.10 (t, 2H, $J_{\mathrm{vic}}=6.6$ Hz), 4.19 (t, 2H, $J_{\mathrm{vic}}=7.2$ Hz), 6.83 (d, 1H, $J_{3,4}=9.0$ Hz), 6.87 (dd, 1H, $J_{4,3}=9.0$, $J_{4,6}=2.9$ Hz), 6.99 ppm (d, 1H, $J_{6,4}=2.9$ Hz); ^{13}C NMR (125.7 MHz, $CDCl_3$, TMS): $\delta=13.58$, 13.60 (2×q), 21.6 (t), 31.7 (t), 34.6 (t), 35.86 (t), 35.94, 35.96, 35.98 (3×t), 67.3 (t), 68.6 (t), 79.5 s), 81.6 (s), 109.2, 109.4, 111.2 (3×s), 112.9 (s), 114.5 (d), 117.1 (d), 119.6 (d), 125.0, 125.2 (2×s), 127.6, 127.7, 127.78, 127.83, 130.4, 130.7 (6×s), 152.3 (s), 154.0 ppm (s); IR (CCl_4): $\tilde{\nu}=3312$, 2961, 2930, 2875, 2860, 2108, 1605, 1580, 1497, 1465, 1380, 1223, 1031 cm^{-1}; UV/Vis ($ClCH_2CH_2Cl$): $\lambda_{\max}$ ($\log\varepsilon$)=219 (4.82), 263 (4.30), 311 (4.39), 329 nm (4.32); MS (TOF MALDI): m/z: 1186 [M^+]; elemental analysis (%) calcd for $C_{48}H_{66}O_2S_{16}$: C 48.52, H 5.60, S 43.18; found: C 48.26, H 5.48, S 42.95.

4,4′-[(2,5-Diiodobenzene-1,4-diyl)bis(oxyethane-2,1-diylsulfanediyl)]-bis[4′,5,5′-tris(butylsulfanyl)-2,2′-bi-1,3-dithiole] (11): A Schlenk flask was charged with tetrathiafulvalene **5** (2.59 g, 4.68 mmol, 2.1 equiv), flushed with argon, and DMF (200 mL) was added. A solution of $CsOH{\cdot}H_2O$ (0.89 g, 5.29 mmol, 2.4 equiv) in methanol (15 mL) was slowly added to the reaction mixture, which was stirred at room temperature for 30 min. Dibromide **7** (1.0 g, 2.23 mmol) dissolved in DMF (50 mL) was added to the reaction mixture, which was further stirred at room temperature for 12 h. The solvent was removed in vacuo, and the crude product was purified by column chromatography on silica gel (chloroform/hexane 60:40) to provide iodide **11** (2.21 g, 70 %) as red crystals. M.p. 73–74 °C (hexane); ^{1}H NMR (600 MHz, $CDCl_3$, TMS): $\delta=0.90$, 0.92, 0.933 (3×t, 18H, $J_{\mathrm{vic}}=7.4$ Hz), 1.37–1.48, 1.56–1.65, 2.79–2.84 (3×m, 36H), 3.19 (t, 4H, $J_{\mathrm{vic}}=6.7$ Hz), 4.13 (t, 4H, $J_{\mathrm{vic}}=6.7$ Hz), 7.19 ppm (s, 2H); ^{13}C NMR (150.9 MHz, $CDCl_3$, TMS): $\delta=13.59$, 13.61, 13.63 (3×q), 21.6 (t), 31.7, 31.75, 31.78 (3×t), 34.8 (t), 35.96, 35.98 (2×t), 69.3 (t), 86.4 (s), 109.5, 111.4 (2×s), 123.4 (d), 124.8 s), 127.6, 127.9, 130.9 (3×s), 152.7 ppm (s); IR (CCl_4): $\tilde{\nu}=2961$, 2932, 2875, 2865, 1594, 1576, 1483, 1465, 1458, 1210 cm^{-1}, UV/Vis ($ClCH_2CH_2Cl$): $\lambda_{\max}$ ($\log\varepsilon$)=248 (4.62), 308 nm (4.52); MS (TOF MALDI): m/z: 1414 [M^+]; MS (TOF ESI+): m/z: 1453 ([M+K]$^+$), 1437 ([M+Na]$^+$), 1414 [M^+]; HRMS (ESI+): m/z calcd for $C_{46}H_{64}O_2I_2NaS_{16}$: 1436.8408 [($M$+Na)$^+$]; found: 1436.8419.

{[4-Iodo-2,5-bis(2-{[4′,5,5′-tris(butylsulfanyl)-2,2′-bi-1,3-dithiol-4-yl]sulfanyl}ethoxy)phenyl]ethynyl}[tris(1-methylethyl)]silane (12) and {[2,5-bis(2-{[4′,5,5′-tris(butylsulfanyl)-2,2′-bi-1,3-dithiol-4-yl]sulfanyl}ethoxy)benzene-1,4-diyl]diethyne-2,1-diyl}bis[tris(1-methylethyl)silane] (13): A Schlenk flask was charged with **11** (3.1 g, 2.19 mmol), [$Pd(PPh_3)_4$] (127 mg, 0.110 mmol, 5 mol %), and CuI (62.6 mg, 0.330 mmol, 15 mol %); flushed with argon; and diisopropylamine (20 mL) and DMF

(20 mL) were added. (Triisopropylsilyl)acetylene (0.536 mL, 2.41 mmol, 1.1 equiv) was added dropwise over 30 min to the reaction mixture, which was stirred at 50 °C for 4 h. The solvent was removed in vacuo, and the crude product was purified by column chromatography on silica gel (chloroform/hexane 70:30) to provide **12** (1.69 g, 45 %) as a red amorphous solid, **13** (1.0 g, 30 %) as an amorphous solid, and recovered starting diiodide **11** (0.65 g, 21 %).

Iodide **12**: ^{1}H NMR (600 MHz, CDCl$_3$, TMS): $\delta=0.89$, 0.915, 0.920, 0.922, 0.925, 0.930 (6×t, 18H, $J_{vic}=7.4$ Hz), 1.14 (m, 21H), 1.36–1.48, 1.55–1.65, 2.79–2.85 (3×m, 36H), 3.14 (t, 2H, $J_{vic}=7.0$ Hz), 3.22 (t, 2H, $J_{vic}=6.6$ Hz), 4.12 (t, 2H, $J_{vic}=7.0$ Hz), 4.14 (t, 2H, $J_{vic}=6.6$ Hz), 6.84 (s, 1H), 7.27 ppm (s, 1H); ^{13}C NMR (150.9 MHz, CDCl$_3$, TMS): $\delta=11.3$ (d), 13.56, 13.59, 13.60, 13.61 (4×q), 18.7 (q), 21.61, 21.63 (2×t), 31.72, 31.74, 31.8 (3×t), 34.7 (t), 35.0 (t), 35.9, 36.0 (2×t), 68.5 (t), 69.2 (t), 87.5 (s), 97.0 (s), 101.8 (s), 109.2, 109.6, 111.2, 111.3 (4×s), 114.3 (s), 117.0 (d), 124.3 (d), 124.8 (s), 125.3 (s), 127.60, 127.63, 127.9, 130.5, 130.7 (5×s), 151.6 (s), 154.5 ppm (s); IR (CCl$_4$): $\tilde{\nu}=2961$, 2931, 2875, 2156, 1587, 1483, 1463, 1373, 1365, 1214, 1023 cm^{-1}; UV/Vis (ClCH$_2$CH$_2$Cl): λ_{max} ($\log\varepsilon$)= 219 (4.05), 270 (4.78), 313 (4.60), 330 nm (4.53); MS (TOF MALDI): m/z: 1468 [M^+]; MS (TOF ESI+): m/z: 1507 ([M+K]$^+$), 1491 ([M+Na]$^+$), 1468 [M^+]; HRMS (ESI+) m/z calcd for $C_{57}H_{85}IO_2NaS_{16}Si$: 1491.0778 [($M$+Na)$^+$]; found: 1491.0787.

Bisethynylated product **13**: ^{1}H NMR (600 MHz, CDCl$_3$, TMS): $\delta=0.90$, 0.918, 0.923 (3×t, 18H, $J_{vic}=7.4$ Hz), 1.15 (m, 42H), 1.37–1.47, 1.56–1.64, 2.82 (3×m, 36H), 3.16 (t, 4H, $J_{vic}=6.9$ Hz), 4.13 (t, 4H, $J_{vic}=6.9$ Hz), 6.88 ppm (s, 2H); ^{13}C NMR (150.9 MHz, CDCl$_3$, TMS): $\delta=11.3$ (d), 13.56, 13.58, 13.59 (3×q), 18.8 (q), 21.59, 21.62, 21.63 (3×t), 31.72, 31.73 (2×t), 34.9 (t), 35.9, 35.96, 35.97 (3×t), 68.3 (t), 97.4 (s), 102.3 (s), 109.3, 111.0 (2×s), 114.6 (s), 117.8 (d), 125.3 (s), 127.6, 127.9, 130.2 (3×s), 153.7 ppm (s); IR (CCl$_4$): $\tilde{\nu}=2961$, 2932, 2875, 2866, 2153, 1603, 1587, 1496, 1465, 1381, 1367, 1221, 1027 cm^{-1}; UV/Vis (ClCH$_2$CH$_2$Cl): λ_{max} ($\log\varepsilon$)=289 (3.85), 334 nm (4.59); MS (TOF MALDI): m/z: 1522 [M^+]; MS (TOF ESI+): m/z: 1461 ([M+K]$^+$), 1445 ([M+Na]$^+$), 1422 [M^+]; HRMS (EI+): m/z calcd for $C_{68}H_{106}O_2NaS_{16}Si_2$: 1545.3155 [($M$+Na)$^+$]; found: 1545.3142.

{[4-{[2,5-Bis(2-{[4′,5,5′-tris(butylsulfanyl)-2,2′-bi-1,3-dithiol-4-yl]sulfanyl}ethoxy)phenyl]ethynyl}-2,5-bis(2-{[4′,5,5′-tris(butylsulfanyl)-2,2′-bi-1,3-dithiol-4-yl]sulfanyl}ethoxy)phenyl]ethynyl}[tris(1-methylethyl)]silane] (14): A Schlenk flask was charged with **12** (837 mg, 0.569 mmol), [Pd(PPh$_3$)$_4$] (98.6 mg, 0.085 mmol, 15 mol %), and CuI (43.4 mg, 0.222 mmol, 40 mol %); flushed with argon; and then a solution of **10** (675 mg, 0.569 mmol, 1.0 equiv) in diisopropylamine (10 mL), DMF (10 mL), and THF (10 mL) was added. The reaction mixture was stirred at room temperature for 3 days. The solvent was removed in vacuo, and the crude product was purified by column chromatography on silica gel (chloroform/ethyl acetate 85:15) to provide **14** (647 mg, 45 %) as a red amorphous solid. ^{1}H NMR (500 MHz, CDCl$_3$, TMS): $\delta=0.86$–0.94 (m, 36H), 1.15 (m, 21H), 1.36–1.48, 1.54–1.66, 2.78–2.85 (3 × m, 72H), 3.12–3.26 (m, 8H), 4.12–4.26 (m, 8H), 6.86 (m, 2H), 6.95 (s, 1H), 7.03 (s, 1H), 7.08 ppm (m, 1H); ^{13}C NMR (125.7 MHz, CDCl$_3$, TMS): $\delta=11.4$ (d), 13.60, 13.62 (2×q), 18.8 (q), 22.7 (t), 31.8 (t), 34.9, 35.0, 35.1, 35.2 (4×t), 35.96, 35.99, 36.00 (3×t), 67.4, 68.3, 68.6, 68.8 (4×t), 89.8 (s), 91.5 (s), 97.6 (s), 104.5 (s), 109.4, 109.5 (2×s), 111.1 (s), 114.2 (s), 114.5 (d), 114.8 (s), 116.9 (d), 117.6 (d), 118.7 (d), 119.0 (d), 125.0, 125.1, 125.4 (3×s), 127.6, 127.8, 127.9, 130.1, 130.4, 130.5 (7×s), 152.5 (s), 153.0 (s), 153.5 (s), 154.0 ppm (s); IR (CCl$_4$,): $\tilde{\nu}=2961$, 2931, 2874, 2865, 2151, 1603, 1579, 1503, 1493, 1465, 1380 cm $^{-1}$; UV/Vis (ClCH$_2$CH$_2$Cl): λ_{max} ($\log\varepsilon$)=226 (4.79), 301 (4.82), 333 nm (4.76); MS (TOF MALDI): m/z: 2526 [M^+].

4-{[2-(2-{[2,5-Bis(2-{[4′,5,5′-tris(butylsulfanyl)-2,2′-bi-1,3-dithiol-4-yl]sulfanyl}ethoxy)phenyl]ethynyl}-5-ethynyl-4-(2-{[4′,5,5′-tris(butylsulfanyl)-2,2′-bi-1,3-dithiol-4-yl]sulfanyl}ethoxy)phenoxy)ethyl]sulfanyl}-4′,5,5′-tris(butylsulfanyl)-2,2′-bi-1,3-dithiole (15): A Schlenk flask was charged with **14** (610 mg, 2.41 mmol), flushed with argon, and a solution of nBu$_4$NF·3H$_2$O (83.8 mg, 0.266 mmol, 1.1 equiv) in THF (15 mL) was added. The reaction mixture was stirred at room temperature for 30 min. The solvent was removed in vacuo, and the crude product was purified by column chromatography on silica gel (chloroform) to provide **15** (561 mg, 98 %) as a red oil. ^{1}H NMR (600 MHz, CD$_2$Cl$_2$): 0.86–0.93 (m, 36H), 1.34–1.48, 1.54–1.64, 2.80–2.84 (3×m, 72H), 3.18 (t, 2H, $J_{vic}=6.5$ Hz), 3.22, 3.242, 3.243 (3×t, 6H, $J_{vic}=6.5$ Hz), 3.40 (s, 1H), 4.14 (t, 2H, $J_{vic}=6.5$ Hz), 4.22, 4.23, 4.24 (3×t, 6H, $J_{vic}=6.5$ Hz), 6.88 (m, 2H), 7.01 (s, 1H), 7.078 (m, 1H), 7.082 ppm (s, 1H); ^{13}C NMR (150.9 MHz, CD$_2$Cl$_2$): $\delta=13.9$, 14.0 (2×q), 22.19, 22.21, 22.23 (3×t), 32.35, 32.40, 32.41 (3×t), 35.6, 35.7 (2×t), 36.51, 36.53, 36.6 (3×t), 68.1 (t), 69.08, 69.11, 69.2 (3×t), 79.9 (s), 83.6 (d), 90.1 (s), 92.3 (s), 109.7, 109.9 (2×s), 113.5 (s), 114.5 (s), 115.4 (d), 115.8 (s), 117.5 (d), 118.2 (d), 119.3 (d), 119.4 (d), 125.99, 126.00, 126.01 (3×s), 128.25, 128.29, 128.32, 128.36, 128.44, 128.5, 130.9, 131.0, 131.1, 131.3 (10×s), 153.2 (s), 153.5 (s), 154.1 (s), 154.4 ppm (s); IR (CCl$_4$): $\tilde{\nu}=$ 3312, 2961, 2932, 2875, 2864, 2418, 1601, 1577, 1495, 1465, 1380, 1221, 1031 cm^{-1}; UV/Vis (ClCH$_2$CH$_2$Cl): λ_{max} ($\log\varepsilon$)=273 (4.69), 298 (4.75), 312 (4.69), 333 nm (4.64); MS (TOF MALDI): m/z: 2370 [M^+].

Acknowledgements

This research was supported by the European Commission under Grant No. FP7-FUNMOL 213382; the Czech Science Foundation under Grant Nos P207/10/2214, 203/09/1802, and 203/09/0705; the Ministry of Education, Youth and Sports of the Czech Republic under Project No. 7E09054; the Grant Agency of the Academy of Sciences of the Czech Republic under Grant No. IAA400400802; and the Institute of Organic Chemistry and Biochemistry, Academy of Sciences of the Czech Republic (RVO: 61388963).

---

[1] a) R. E. Martin, F. Diederich, *Angew. Chem.* **1999**, *111*, 1440–1469; *Angew. Chem. Int. Ed.* **1999**, *38*, 1350–1377; b) Y. Geerts, G. Klärner, K. Müllen in *Electronic Materials: The Oligomer Approach* (Eds.: K. Müllen, G. Wegner), Wiley-VCH, Weinheim, **1998**, pp. 1–103.

[2] R. Chinchilla, C. Nájera, *Chem. Rev.* **2007**, *107*, 874–922.

[3] J. M. Tour, *Acc. Chem. Res.* **2000**, *33*, 791–804.

[4] a) J. M. Tour, *Molecular Electronics*, World Scientific, Singapore, **2003**; b) U. H. F. Bunz, *Chem. Rev.* **2000**, *100*, 1605–1644.

[5] a) A. Godt, M. Schulte, H. Zimmermann, G. Jeschke, *Angew. Chem.* **2006**, *118*, 7722–7726; *Angew. Chem. Int. Ed.* **2006**, *45*, 7560–7564; b) P. F. H. Schwab, M. D. Levin, J. Michl, *Chem. Rev.* **1999**, *99*, 1863–1933.

[6] According to the REAXYS database: C. Xue, F.-T. Luo, *Tetrahedron* **2004**, *60*, 6285–6294.

[7] For illustrative recent examples, see: a) J. R. Acharya, H. Zhang, X. Li, E. E. Nesterov, *J. Am. Chem. Soc.* **2009**, *131*, 880–881; b) T. Yatabe, Y. Suzuki, Y. Kawanishi, *J. Mater. Chem.* **2008**, *18*, 4468–4477.

[8] For illustrative examples, see: a) K.-Y. Pu, X.-Y. Qi, Y.-L. Yang, X.-M. Lu, T.-C. Li, Q.-L. Fan, C. Wang, B. Liu, H. S. O. Chan, W. Huang, *Chem. Eur. J.* **2008**, *14*, 1205–1215; b) Y. Yamaguchi, T. Tanaka, S. Kobayashi, T. Wakamiya, Y. Matsubara, Z.-I. Yoshida, *J. Am. Chem. Soc.* **2005**, *127*, 9332–9333.

[9] For an illustrative example, see: J.-J. Hwang, J. M. Tour, *Tetrahedron* **2002**, *58*, 10387–10406.

[10] For illustrative examples, see: a) A. Blaszczyk, M. Fischer, C. von Haenisch, M. Mayor, *Eur. J. Org. Chem.* **2007**, 2630–2642; b) M. Kozaki, K. Okada, *Org. Lett.* **2004**, *6*, 485–488.

[11] For illustrative recent examples, see: a) J. Tolosa, C. Kub, U. H. F. Bunz, *Angew. Chem.* **2009**, *121*, 4680–4682; *Angew. Chem. Int. Ed.* **2009**, *48*, 4610–4612; b) S. Grunder, R. Huber, V. Horhoiu, M. T. Gonzalez, C. Schoenenberger, M. Calame, M. Mayor, *J. Org. Chem.* **2007**, *72*, 8337–8344.

[12] For illustrative examples, see: a) A. Al Ouahabi, P. N. W. Baxter, J.-P. Gisselbrecht, A. De Cian, L. Brelot, N. Kyritsakas-Gruber, *J. Org. Chem.* **2009**, *74*, 4675–4689; b) J. A. Marsden, J. J. Miller, L. D. Shirtcliff, M. M. Haley, *J. Am. Chem. Soc.* **2005**, *127*, 2464–2476.

[13] For illustrative recent examples, see: a) T. Ochi, Y. Yamaguchi, T. Wakamiya, Y. Matsubara, Z.-I. Yoshida, *Org. Biomol. Chem.* **2008**,

6, 1222–1231; b) T. Ochi, Y. Yamaguchi, S. Kobayashi, T. Wakamiya, Y. Matsubara, Z.-I. Yoshida, *Chem. Lett.* **2007**, *36*, 794–795.

[14] For illustrative examples, see: a) G. Mao, A. Orita, D. Matsuo, T. Hirate, J. Otera, T. Iwanaga, S. Toyota, *Tetrahedron Lett.* **2009**, *50*, 2860–2864; b) H.-C. Zhang, L. Pu, *Macromolecules* **2004**, *37*, 2695–2702.

[15] For illustrative examples, see: a) K. Walzer, E. Marx, N. C. Greenham, R. J. Less, P. R. Raithby, K. Stokbro, *J. Am. Chem. Soc.* **2004**, *126*, 1229–1234; b) M. P. Stewart, F. Maya, D. V. Kosynkin, S. M. Dirk, J. J. Stapleton, C. L. McGuiness, D. L. Allara, J. M. Tour, *J. Am. Chem. Soc.* **2004**, *126*, 370–378.

[16] For illustrative recent examples, see: a) G. K. B. Clentsmith, L. D. Field, B. A. Messerle, A. Shasha, P. Turner, *Tetrahedron Lett.* **2009**, *50*, 1469–1471; b) L.-G. Wang, Z.-T. Li, *Synlett* **2009**, 384–389.

[17] For illustrative recent examples, see: a) L. Liu, C.-H. Sue, J. F. Stoddart, Y.-L. Zhao, W. Zhang, Q. Li, O. S. Miljanic, O. M. Yaghi, *Chem. Eur. J.* **2009**, *15*, 13356–13380; b) H. Tsuji, C. Mitsui, L. Ilies, Y. Sato, E.-I. Nakamura, *J. Am. Chem. Soc.* **2007**, *129*, 11902–11903.

[18] For illustrative recent examples, see: a) C.-H. Zhao, E. Sakuda, A. Wakamiya, S. Yamaguchi, *Chem. Eur. J.* **2009**, *15*, 10603–10612; b) C.-H. Zhao, A. Wakamiya, Y. Inukai, S. Yamaguchi, *J. Am. Chem. Soc.* **2006**, *128*, 15934–15935.

[19] For an illustrative example, see: J.-F. Nierengarten, S. Zhang, A. Gegout, M. Urbani, N. Armaroli, G. Marconi, Y. Rio, *J. Org. Chem.* **2005**, *70*, 7550–7557.

[20] For illustrative recent examples, see: a) J. Fortage, J. Boixel, E. Blart, F. Odobel, L. Hammarstroem, H. C. Becker, *Chem. Eur. J.* **2008**, *14*, 3467–3480; b) Y. Yamamoto, K. Hattori, *Tetrahedron* **2008**, *64*, 847–855.

[21] For an illustrative example, see: A. S. Droz, U. Neidlein, S. Anderson, P. Seiler, F. Diederich, *Helv. Chim. Acta* **2001**, *84*, 2243–2289.

[22] For an illustrative example, see: J. K. Sørensen, M. Vestergaard, A. Kadziola, K. Kilsa, M. B. Nielsen, *Org. Lett.* **2006**, *8*, 1173–1176.

[23] *Handbook of Conducting Polymers, 3rd ed.* (Eds.: T. A. Skotheim, J. Reynolds), CRC, Boca Raton, **2007**.

[24] For the phosphonate group, see: a) M. R. Pinto, B. M. Kristal, K. S. Schanze, *Langmuir* **2003**, *19*, 6523–6533; for the sulfonate or bis-alkylammonium groups, see: b) X. Zhao, M. R. Pinto, L. M. Hardison, J. Mwaura, J. Müller, H. Jiang, D. Witker, V. D. Kleiman, J. R. Reynolds, K. S. Schanze, *Macromolecules* **2006**, *39*, 6355–6366.

[25] G. M. Farinola, F. Babudri, A. Cardone, O. H. Omar, F. Naso, *Pure Appl. Chem.* **2008**, *80*, 1735–1746.

[26] a) B. M. Illescas, J. Santos, C. M. Atienza, N. Martin, M. Wielopolski, D. M. Guldi, *Chem. Commun.* **2009**, 5374–5376; b) M. Wielopolski, C. Atienza, T. Clark, D. M. Guldi, N. Martín, *Chem. Eur. J.* **2008**, *14*, 6379–6390; c) Y. Hou, Y. Chen, Q. Liu, M. Yang, X. Wan, S. Yin, A. Yu, *Macromolecules* **2008**, *41*, 3114–3119; d) Y. Liu, A. H. Flood, P. A. Bonvallet, S. A. Vignon, B. H. Northrop, H.-R. Tseng, J. O. Jeppesen, T. J. Huang, B. Brough, M. Baller, S. Magonov, *J. Am. Chem. Soc.* **2005**, *127*, 9745–9759.

[27] a) R. Bhosale, J. Míšek, N. Sakai, S. Matile, *Chem. Soc. Rev.* **2010**, *39*, 138–149; b) S. Maity, R. Bhosale, N. Banerji, E. Vauthey, N. Sakai, S. Matile, *Org. Biomol. Chem.* **2010**, *8*, 1052–1057; c) N. Sakai, R. Bhosale, D. Emery, J. Mareda, S. Matile, *J. Am. Chem. Soc.* **2010**, *132*, 6923–6925.

[28] a) G. Gilli, P. Gilli, *The Nature of the Hydrogen Bond: Outline of a Comprehensive Hydrogen Bond Theory*, Oxford University Press, New York, **2009**; b) *Supramolecular Assembly via Hydrogen Bonds I* (Ed.: D. M. P. Mingos), Springer, Berlin, **2004**; c) G. A. Jeffrey, *An Introduction to Hydrogen Bonding*, Oxford University Press, New York, **1997**.

[29] F. Wudl, G. M. Smith, E. J. Hufnagel, *J. Chem. Soc. D* **1970**, 1453–1454.

[30] a) *TTF Chemistry: Fundamentals and Applications of Tetrathiafulvalene* (Eds.: J.-I. Yamada, T. Sugimoto), Kodansha Springer, Berlin, **2004**; b) M. Bendikov, F. Wudl, D. F. Perepichka, *Chem. Rev.* **2004**, *104*, 4891–4946.

[31] a) D. Canevet, M. Salle, G. X. Zhang, D. Q. Zhang, D. B. Zhu, *Chem. Commun.* **2009**, 2245–2269; b) K. A. Nielsen, E. Levillain, V. M. Lynch, J. L. Sessler, J. O. Jeppesen, *Chem. Eur. J.* **2009**, *15*, 506–516; c) M. B. Nielsen, C. Lomholt, J. Becher, *Chem. Soc. Rev.* **2000**, *29*, 153–164.

[32] A. Saad, F. Barrière, E. Levillain, N. Vanthuyne, O. Jeannin, M. Fourmigué, *Chem. Eur. J.* **2010**, *16*, 8020–8028.

[33] V. Khodorkovsky, L. Shapiro, P. Krief, A. Shames, G. Mabon, A. Gorguesc, M. Giffard, *Chem. Commun.* **2001**, 2736–2737.

[34] S. V. Rosokha, J. K. Kochi, *J. Am. Chem. Soc.* **2007**, *129*, 828–838.

[35] a) V. Maurizot, M. Yoshizawa, M. Kawano, M. Fujita, *Dalton Trans.* **2006**, 2750–2756; b) M. Yoshizawa, K. Kumazawa, M. Fujita, *J. Am. Chem. Soc.* **2005**, *127*, 13456–13457; c) A. Y. Ziganshina, Y. H. Ko, W. S. Jeon, K. Kim, *Chem. Commun.* **2004**, 806–807.

[36] a) A. Coskun, J. M. Spruell, G. Barin, A. C. Fahrenbach, R. S. Forgan, M. T. Colvin, R. Carmieli, D. Benítez, E. Tkatchouk, D. C. Friedman, A. A. Sarjeant, M. R. Wasielewski, W. A. Goddard III, J. F. Stoddart, *J. Am. Chem. Soc.* **2011**, *133*, 4538–4547; b) K.-I. Nakamura, T. Takashima, T. Shirahata, S. Hino, M. Hasegawa, Y. Mazaki, Y. Misaki, *Org. Lett.* **2011**, *13*, 3122–3125; c) V. A. Azov, R. Gómez, J. Stelten, *Tetrahedron* **2008**, *64*, 1909–1917; d) I. Aprahamian, J.-C. Olsen, A. Trabolsi, J. F. Stoddart, *Chem. Eur. J.* **2008**, *14*, 3889–3895; e) M. Iyoda, M. Hasegawa, Y. Miyake, *Chem. Rev.* **2004**, *104*, 5085–5113; f) J. O. Jeppesen, M. B. Nielsen, J. Becher, *Chem. Rev.* **2004**, *104*, 5115–5131.

[37] P.-T. Chiang, N.-C. Chen, C.-C. Lai, S.-H. Chiu, *Chem. Eur. J.* **2008**, *14*, 6546–6552.

[38] a) M. Rahimizadeh, E. R. Seresht, N. Golari, M. Bakavoli, *Monatsh. Chem.* **2008**, *139*, 639–645; b) P. R. Ashton, S. E. Boyd, C. G. Claessens, R. E. Gillard, S. Menzer, J. F. Stoddart, M. S. Tolley, A. J. P. White, D. J. Williams, *Chem. Eur. J.* **1997**, *3*, 788–798; c) R. Adams, L. N. Whitehill, *J. Am. Chem. Soc.* **1941**, *63*, 2073–2078.

[39] J. Rybáček, M. Rybáčková, M. Høj, M. Bělohradský, P. Holý, K. Kilså, M. B. Nielsen, *Tetrahedron* **2007**, *63*, 8840–8854.

[40] M. Giffard, P. Alonso, J. Garín, A. Gorgues, T. P. Nguyen, P. Richomme, A. Robert, J. Roncali, S. Uriel, *Adv. Mater.* **1994**, *6*, 298–300.

[41] A. J. Bard, L. R. Faulkner, *Electrochemical Methods, Fundamentals and Applications*, Wiley, New York, **2001**, Chap. 6.7.

[42] P. A. Malachesky, *Anal. Chem.* **1969**, *41*, 1493–1494.

[43] R. Pou-Amérigo, E. Ortí, M. Merchán, M. Rubio, P. M. Viruela, *J. Phys. Chem. A* **2002**, *106*, 631–640.

[44] a) M. Giffard, G. Mabon, E. Leclair, N. Mercier, M. Allain, A. Gorgues, P. Molinié, O. Neilands, P. Krief, V. Khodorkovsky, *J. Am. Chem. Soc.* **2001**, *123*, 3852–3853; b) M. González, B. Illescas, N. Martín, J. L. Segura, C. Seoane, M. Hanack, *Tetrahedron* **1998**, *54*, 2853–2866.

[45] a) M. Frei, F. Diederich, R. Tremont, T. Rodríguez, L. Echegoyen, *Helv. Chim. Acta* **2006**, *89*, 2040–2057; b) J. Lyskawa, M. Sallé, J.-Y. Balandier, F. Le Derf, E. Levillain, M. Allain, P. Viel, S. Palacin, *Chem. Commun.* **2006**, 2233–2235; c) S. Bouguessa, K. Hervé, S. Golhen, L. Ouahab, J.-M. Fabre, *New J. Chem.* **2003**, *27*, 560–564; d) F. Le Derf, E. Levillain, G. Trippé, A. Gorgues, M. Sallé, R.-M. Sebastian, A.-M. Caminade, J.-P. Majoral, *Angew. Chem.* **2001**, *113*, 230–233; *Angew. Chem. Int. Ed.* **2001**, *40*, 224–227; e) H. Spanggaard, J. Prehn, M. B. Nielsen, E. Levillain, M. Allain, J. Becher, *J. Am. Chem. Soc.* **2000**, *122*, 9486–9494; f) P. Blanchard, N. Svenstrup, J. Becher, *Chem. Commun.* **1996**, 615–616; g) M. Jørgensen, K. A. Lerstrup, K. Bechgaard, *J. Org. Chem.* **1991**, *56*, 5684–5688.

[46] Gaussian 09 (Revision A.1), M. J. Frisch, G. W. Trucks, H. B. Schlegel, G. E. Scuseria, M. A. Robb, J. R. Cheeseman, G. Scalmani, V. Barone, B. Mennucci, G. A. Petersson, H. Nakatsuji, M. Caricato, X. Li, H. P. Hratchian, A. F. Izmaylov, J. Bloino, G. Zheng, J. L. Sonnenberg, M. Hada, M. Ehara, K. Toyota, R. Fukuda, J. Hasegawa, M. Ishida, T. Nakajima, Y. Honda, O. Kitao, H. Nakai, T. Vreven, J. A. Montgomery, Jr., J. E. Peralta, F. Ogliaro, M. Bearpark, J. J. Heyd, E. Brothers, K. N. Kudin, V. N. Staroverov, R. Kobayashi, J. Normand, K. Raghavachari, A. Rendell, J. C. Burant, S. S. Iyengar, J. Tomasi, M. Cossi, N. Rega, J. M. Millam, M. Klene, J. E. Knox, J. B. Cross, V. Bakken, C. Adamo, J. Jaramillo, R. Gomperts, R. E. Stratmann, O. Yazyev, A. J. Austin, R. Cammi, C. Pomelli, J. W.

Ochterski, R. L. Martin, K. Morokuma, V. G. Zakrzewski, G. A. Voth, P. Salvador, J. J. Dannenberg, S. Dapprich, A. D. Daniels, Ö. Farkas, J. B. Foresman, J. V. Ortiz, J. Cioslowski, D. J. Fox, Gaussian, Inc., Wallingford CT, **2009**.

[47] a) J. Vacek, J. Michl, *New J. Chem.* **1997**, *21*, 1259–1267; b) J. Vacek, J. Michl, *Proc. Natl. Acad. Sci. USA* **2001**, *98*, 5481–5486.

[48] A. K. Rappé, C. J. Casewit, K. S. Colwell, W. A. Goddard III, W. M. Skiff, *J. Am. Chem. Soc.* **1992**, *114*, 10024–10039.

[49] A. K. Rappé, W. A. Goddard III, *J. Phys. Chem.* **1991**, *95*, 3358–3363.

[50] The software used for the simulation of electrochemical experiments was ESP package written by Dr. C. Nervi (available at http://lem.ch.unito.it/chemistry/electrochemistry.html).

[51] Under some circumstances, the height of a cyclic voltammogram redox wave can be smaller than expected (not reflecting the number of transferred electrons), which may occur, for example, if the electrochemical redox step is preceded with a slower nonelectrochemical equilibration; for details, see ref. [36a].

Received: September 13, 2011
Revised: January 8, 2013